

FLUORESCENCE AND FIBER-OPTICS BASED REAL-TIME THICKNESS SENSOR FOR DYNAMIC LIQUID FILMS

T. W. Ng and A. Narain (E-mail: narain@mtu.edu)

Department of Mechanical Engineering-Engineering Mechanics
Michigan Technological University
Houghton, MI-49931

ABSTRACT

To overcome the limitations/disadvantages of many known liquid film thickness sensing devices (viz. conductivity probes, reflectance based fiber-optics probes, capacitance probes, etc.), a new liquid film thickness sensor that utilizes fluorescence phenomena and fiber-optic technology has been developed and reported here. Measurements from this sensor are expected to facilitate better understanding of liquid film dynamics in various adiabatic, evaporating, and condensing film flows.

The sensor accurately measures the instantaneous thickness of a dynamically changing liquid film in such a way that the probe does not perturb the flow dynamics in the proximity of the probe's tip. This is achieved by having the probe's exposed surface embedded flush with the surface over which the liquid film flows, and by making arrangements for processing the signals associated with the emission and collection of light (in distinctly different wavelength windows) at the probe's flush surface. Instantaneous film thickness in the range of 0.5 to 3.0 mm can accurately (with a resolution that is within +/- 0.09 mm over 0.5 to 1.5 mm range and within +/- 0.18 mm over 1.5 to 3.0 mm range) be measured by the sensor described in this paper. Although this paper only demonstrates the sensor's ability for dynamic film thickness measurements carried out for a doped liquid called FC-72 (perfluorohexane or C_6F_{14} from 3M Corporation), the approach and development/calibration procedure described here can be extended, under similar circumstances, to some other liquid films as well.

1. INTRODUCTION

Over the last few decades, measurement of a dynamic liquid film's thickness has become increasingly important in numerous research and development fields. This paper focuses on a sensor capable of measuring interfacial wave characteristics – such as the content of amplitude, frequency and propagation velocity (by post processing film thickness data at known locations) that could be obtained from analyzing film thickness measurements at different “points.” This is for applications where an understanding of interfacial wave characteristics is important - either by itself or because of its relationship to interfacial mass and heat transfer rates. Need for such measurements based information exists for various two-phase systems that involve film flows under adiabatic, evaporating, or condensing conditions.

To achieve the goal of accurately measuring liquid film thickness values (instantaneous or time averaged), many techniques have been developed to satisfy the measurement objectives within the framework of experimental goals, constraints, and equipment restrictions imposed by the specific needs of the application of interest. These techniques include the use of electrical conductivity [1] or capacitance [2] measurements

and correlating the measurements to the thickness of the liquid film. In the present context of measurements, a well known distance measuring principle was employed [3] by a flush probe that emitted ultrasound waves and collected/analyzed the incident reflected waves to identify and measure the total transit time of the sound wave (of known wave-speed) – and thus thickness (obtained by multiplying the wave speed by half of the transit time) - as waves travelled from the flush probe to the film interface and then returned from the interface after its first reflection. Use of optical reflection from the liquid film's interface [4-7], optical interference [8-10] of illuminating and reflecting lights, optical ellipsometry [11-12], optical absorption/transmission [13-14] characteristics, optical fluorescence imaging [15-18] of the liquid film, and the approach of measuring the amount of fluorescent light (see [19-20] as well as the approach described in this paper) are all optical techniques that are known to be reasonably successful within their respective context and purpose. As expected, direct mechanical measurements involving needle contact [21] have been used very early on for scientific studies where the intrusion of the probe in the film does not lead to significant alteration of the flow.

Among the above, conductivity and capacitance measurements based approaches for a liquid film's thickness are the most popular among the non-intrusive techniques. These techniques utilize a one or two electrode probes [1-2] that are mounted flush or close to the surface on which the liquid flows and they measure the conductance and capacitance of a certain volume of the liquid film (which depends on film thickness) in the vicinity of the probe. However, a major limitation of these [1-2] as well as the ultrasound [3] approaches are their insufficient spatial resolution which makes their use undesirable when a spatially non-uniform and time varying thickness needs to be dynamically resolved. In case of the presence of waves and interest in their characteristics, these methods typically do not yield anything more than spatially averaged values of local film thickness.

All optical approaches, including the one proposed here, typically require a transparent liquid film. However methods based on optical reflection and optical interference techniques depend on the exciting light's reflection from the liquid interface and hence they do not work well in the presence of waves on the liquid's interface. These techniques, then, are only useful for relatively accurate thickness measurements of very thin films (within nano- to micron- scale) - where wave effects are negligible.

In summary, many liquid film thickness measuring techniques have been developed, each with its own range of applicability, advantages, disadvantages, and limitations. However, for characterizing wave motions on dynamic liquid films of thickness in the range of 0.2 mm to 5 mm, available sensors show limitations and/or a need for additional enhancements/modifications.

A sensor based on the laser-induced fluorescence principle (as in [19]) was chosen in the context of favourable changes in the availability of relevant modern technology and towards addressing: (i) the need for good *local* and *real-time* film thickness measurements in the presence of interfacial waves - as opposed to typical spatial and temporal averaging over unacceptably large volumes and/or time-intervals, (ii) the need for a non-intrusive technique that does not alter the wave characteristics, and (iii) the need for viability of the measurement technique for situations where the liquid film of interest flows on the surface of an opaque metal

and one's optical access to the flow is limited to what is feasible by fiber-optics. The technique and principles developed in this paper meets these requirements and the rest of the paper describes the development of a sensor which innovatively exploits the known principle of fluorescence in this specific context.

2. PRINCIPLE OF THE SENSOR

The above stated goal is to have the sensing probe accurately measure instantaneous thickness of a dynamically changing liquid film in such a way that the probe does not perturb the flow phenomenology in the proximate distance to the probe's tip. This is achieved by having the probe's exposed surfaces embedded flush with the flow surface (the surface on which the liquid film flows or moves) and processing the signals associated with light emission and light collection at the probe's flush surfaces. A thickness range between 0.5 to 3.0 mm is resolved by the developed sensor.

Film thickness measurements are carried out for stationary and dynamic films of a liquid called FC-72 (perfluorohexane or C_6F_{14} made by 3M Corporation). The liquid film shown in Figure 1 is fluoresced by exciting it with a suitable light source. A portion of the fluorescent light – which has a different and distinct wavelength spectrum than the spectrum of the excitation light - falls back on a designated collection area of the flush probe. As shown in Fig. 2, the flush probe in Fig. 1 has an arrangement of illumination (marked I) and collection (marked R) locations where the fiber-optic cables' tips-with-filters (i.e. tips that end at suitably small and thin optical filters) are flush with the sensor's probe area. The amount of collected/detected fluorescent light depends, among other variables, on the instantaneous film thickness to be measured. By the calibration technique described here, the measured value of the detected fluorescent light correlates directly to the instantaneous film thickness.

To fluoresce the liquid film, the FC-72 is slightly doped (concentration = mass of dopant * 100 / mass of total solution = 0.20%) by a suitably chosen fluorescent additive (bi-acetyl or $C_4H_6O_2$ in this case). The excitation of this doped liquid film at shorter wavelengths of light (400-410 nm) leads to sufficient absorption of this light. This, in turn, induces sufficient fluorescent emission at longer wavelengths (460-600 nm). In other words, molecular absorption of shorter-wavelength photons triggers emission of lower-energy photons with longer wavelengths. The wavelength spectrum of emitted fluorescent light (460-600 nm) is separated and identified for detection because light in this spectrum - as it traverses its way out of this film - is not self-quenched, or absorbed by the doped liquid film. The excitation light is arranged to be minuscule in order to excite the film mostly through the primary illumination cone of Fig. 3 (i.e., to minimize presence of secondary illumination cones resulting from interfacial reflection of the excitation light in the primary illumination cone) and, *also*, to avoid crossing a certain threshold level of detected fluorescent light that is actually unwanted because it arrives at the sensor's axially symmetric collection area indirectly - after its reflection from the interface of the liquid film. As a result of the minuscule excitation, the detected light (after filtering out the excitation light) in the fluorescent range is also minuscule and is detected by a sensitive photo-multiplier tube. The *predominant* amount of detected light comes directly from the fluorescent light originating in the primary illumination cone of Fig. 3, and a much smaller amount comes indirectly – after its interfacial reflection. This

predominant component of detected light correlates directly with instantaneous film thickness and is actually made precisely known (and deterministic) - by a process of sorting and identifying this portion of the total detected light with the help of a paired set of calibration experiments especially developed for this purpose. The results of the calibration experiments, as well as experimental demonstration of the sensor's dynamic measurement capabilities, are reported in this paper.

Choice of Dopant

The pure working liquid FC-72 is a clear, colorless and odorless dielectric liquid with high density, low viscosity, low surface tension, and low boiling point (56°C at one atmospheric pressure). It is commonly used as an electronic cooling fluid due to its low boiling point, high convective heat transfer coefficient, and its clean, safe and easy-to-use characteristics. It has a spectral absorptivity of nearly zero over the visible range. Here FC-72 is doped by dissolving a small amount of bi-acetyl, $C_4H_6O_2$ (henceforth called dopant). It has been verified through separate experiments in a transparent distillation apparatus that this dopant evaporates and condenses together with FC-72.

The doped FC-72 solution, when excited by a 408 nm laser source, results in significant absorbance and sufficient fluorescence of the bi-acetyl molecules. The solution's absorbance and fluorescence characteristics are shown in Figures 4 and 5 respectively. In Figure 4, absorbance = 0 has been set for pure FC-72. The fluorescent light of interest is in a wavelength zone ($460 \text{ nm} \leq \lambda \leq 600 \text{ nm}$) that is sufficiently apart and different from the excitation laser light's wavelengths that are narrowly distributed around 408 nm. This spectral zone of fluorescent light is separated out, from all the other light present, with the help of suitable filters. These filters block almost all the ambient and noise light present outside this spectral zone. The total amount of light in the fluorescent zone is then detected by a photo-detector. It is shown in this paper that, for fixed optical/electrical settings of the employed hardware and a known concentration of a doped solution, the filtered and detected fluorescent light can be correlated with the instantaneous film thickness, d , of the primary illumination zone (see Figure 3).

The measurements reported in Figure 4 were done with a 10 mm light path cuvette in a Beckman Spectral Photometer. The concentration ($C = \text{mass of bi-acetyl} * 100 / \text{total mass of solution}$) of the doped solution was 0.121%. It is seen through the absorbance spectrum (see Figure 4) that the detected fluorescent light ($470 \text{ nm} \leq \lambda \leq 600 \text{ nm}$), when making its way out of the liquid film, will see zero absorbance and hence will not be self-quenched or absorbed by the liquid film.

For an excitation light of $\lambda = 425 \text{ nm}$, in Figure 5, the dashed curve indicates the level of fluorescence (dominant over 460 to 600 nm range) that the doped solution yields. This curve was obtained by a fluorescence meter (Fluorolog; 250 W Xenoxlamp) when a doped solution ($C = 0.054\%$) was excited by a 425 nm light source. The solid curve plots the "factor" ($0 \leq \text{factor} \leq 1.02$) by which the dashed curve (i.e. fluorescent spectrum obtained with 425 nm excitation) values must be multiplied to predict fluorescence if the excitation light's wavelength is different than $\lambda = 425 \text{ nm}$. This scaling factor, as can be seen by comparison of the solid curve in Fig. 5 with the curve in Fig. 4, is proportional to the absorbance of the doped solution.

For instance, to obtain the fluorescent spectrum at any excitation $\lambda \neq 425$ nm, one should multiply the reported fluorescent spectrum's intensity (photon counts over instrument's specified interval of time) by the indicated scaling factor given by the solid curve in Fig. 5.

3. REQUIREMENTS

Based on the above discussions of the sensor principle, and our experience with the sensor, this film thickness sensor can be used whenever the following requirements are met:

- The liquid film whose thickness is to be measured transmits light and can, if needed, be doped by a fluorescent chemical. If doping is not allowed in the real process, it is assumed that it is allowed in a prototypical process. The absorbance and fluorescence spectrum of the doped liquid must meet the criteria discussed under "choice of dopant".
- The measurement can take place either in a dark environment with no ambient light or only under an ambient light illumination at selected and allowable wavelengths that do not interfere with wavelengths associated with excitation or collection lights.
- The inner walls of the container, within which flow of the film takes place, must be close to a "black surface" to minimize reflection of the excitation light.
- The components of the sensor and the sensing environment must be clean to avoid autofluorescence (caused by excitation light) from impurities that can corrupt the signal in the spectrum of the light to be sensed.
- The liquid film thickness should be within a certain well defined range (which is 0.5 mm to 3.0 mm for the reported situation). A wider range for measurements is possible if sensor arrangement is suitably modified.

4. SENSOR SCHEMATIC, HARDWARE, AND EXPERIMENTAL PROCEDURE

4.1 Schematic

The schematic of the experimental setting of the developed sensor is depicted in Figure 6. In general, illuminating light from a 408 nm violet laser source is transmitted through fiber I of a core diameter of 200 μm . The light coming out of the fiber I illuminates a nearly cylindrical primary cone within a stationary or dynamic film (made up of a bi-acetyl doped FC-72 liquid). For the reported experiments, this liquid film is inside a cylindrical anodized aluminum container. Absorption of the violet photons by the dopant molecules is followed, in less than a nano second, by an emission of photons in longer-wavelengths, which are within the range of 470 to 600 nm. It should be noted that previous spectrofluorometer experiments have confirmed that no fluorescence is yielded if pure FC-72 liquid is subjected to this excitation. The doped solution's fluorescent light ranging within 470 to 600 nm is channeled through a set of other optical fibers R (which are chosen to have a bigger core diameter of 800 μm and are arranged as in Fig. 2) into a photo-detector of choice (which is, under actual conditions, a photomultiplier tube). The detector in Fig. 6 indicates use of either a spectrometer

or a photomultiplier tube/that is connected to an oscilloscope. The spectrometer is only used for ascertaining the spectral content of detected light during evaluation of the system performance – which is typically done at illumination light levels that are kept artificially higher than those used for calibration experiments or actual use of the sensor.

Along the optical paths, installation of the optical filters is needed to minimize the presence of noise light within the detected fluorescent range of interest. For instance, a short-pass (SP) filter, which allows transmission of light with wavelengths shorter than a specific wavelength λ , needs to be installed at filter holder F1 in Figure 6. This SP filter allows wavelengths below 415 nm to pass and blocks the very small noise light (see Fig. 7b), in the range of 420 to 700 nm, which typically accompanies the violet excitation laser light's spectrum shown in Fig. 7a. Figure 7c indicates the smallness of the total optical output associated with representative spectrums in Fig. 7a – this follows from the fact that typical calibration experiments are done close to the lower threshold of 40 mA in Fig. 7c. Experiments in this paper show that, even though the noise magnitude is insignificant when compared to the *relatively* strong violet excitation light (i.e. a logarithmic ratio of 100:10000 or 1:100), the noise light can be strong relative to the extremely low value of the desired signal (the fluorescent light to be detected) – all this resulting in a poor signal-to-noise ratio.

Additionally, a short pass filter (blocks all light above $\lambda \geq 420$ nm) is employed at the tip of the illuminating fiber I in Fig. 6. The purpose of this filter is to reduce noise light that goes through, despite the presence of the filter at F1, and, also, to eliminate some noise light that is created by the auto-fluorescence of the illuminating fiber I. In addition to the above, between F1 and the exit of the laser-diode (LD)-to-fiber coupler, more ultra-thin SP filters are placed to further improve the ability to block any undesired noise light arising from auto-fluorescence of the optical components inside the coupler.

A long-pass (LP) filter, which allows transmission of light of wavelengths longer than a specific wavelength $\lambda = 470$ nm, is installed at filter holder F2 right before the photo-detector to block any persistent 408 nm excitation light (despite filtering at R-tip) that enters the receiving fibers after its reflection from the liquid-vapor interface, and, possibly, from the black-surface (or blackbody cavity) of the container walls above and around the interface. This filtering is especially required when a photomultiplier tube is utilized for photo-detection since the reflected light has the potential of over-saturating the detector as the light can be strong relative to the fluorescent light. Identical LP filters, which block wavelengths below 470 nm, are also placed on the tips of the receiving fibers R. These filters allow the desired fluorescent light (within wavelengths of 470 to 600 nm) to be carried through R but are able to block/reduce the amount of 408 nm excitation laser light that would otherwise enter R and possibly cause auto-fluorescence (in the spectrum of interest) from certain materials between R and the detector.

4.2 Hardware Implementation and Experimental Procedure

A system consisting of optical, electrical, and mechanical subsystems has been developed for the sensor. This section gives an overall picture of how hardware components are integrated into three optical subsystems which are: laser diode-to-fiber coupler used for laser illumination and focusing onto the illuminating fiber,

illuminating (laser light) and receiving fibers with their associated filters and fittings, and photodetector for fluorescent light with its associated filter and adapter. Figures 6 and 8 respectively present the schematic design and the actual physical assemblies of the overall system. Additional details of all the pieces of hardware – including optical, electrical, and mechanical components - are given in Ng [22].

4.2.1 Laser Illumination and Focusing onto the Illuminating Fiber

A violet laser diode (LD) is installed in a laser-to-fiber coupler. Violet light illuminated by the LD is collimated by a collimating lens and then filtered through some 4*4 mm square 300 μm thin 415 nm short-pass (SP) filters (transmit nearly all wavelengths shorter than 415 nm) to block all laser background noise. To monitor laser power of the LD so as to ensure constancy of the light output, a 50 μm core multimode (MM) fiber is connected to the side path, shown in Fig. 6 as beam pick-off fiber, of the laser-to-fiber coupler. Some 4-8% of the laser light is captured through a beam splitter and channeled through this 50 μm core fiber. A photodiode and an oscilloscope are used to detect the light coming out of this beam sampler. The filtered light is focused by an aspheric lens into a 200 μm core fiber. In addition, one thermoelectric cooler is connected to the photodiode and one to the laser-to-fiber coupler to maintain each one of them at specified constant temperatures (of 20°C). This ensures the stability and consistency of the devices' performance. An extra fan acting as a heat sink is also attached onto the laser-to-fiber coupler to allow better heat dissipation during the LD operation.

Several laser diode (LD) operating precautions need to be followed for proper operation of the LD. These precautions include: staying within specified LD current limits, operating at a fixed LD temperature, LD grounding and cable fastening, physical separation of the LD from other electronics and cables, and LD handling and transporting. All ESD (electrostatic discharge) sensitive electronics are placed on top of a grounded, anti-static table mat. Any electrical and optical cables, which are sensitive to physical arrangement and/or movement, must also be properly secured. Filter placements at different locations (e.g. inside the laser-to-fiber coupler, before the photomultiplier tube or spectrometer, and on the tips of the optical fibers) need to be done with care to ensure sufficient rigidity. Fiber mounting on the calibrating container and its bonding with the container is done with the help of a non-fluorescent black silicone. Flush mounting the probe in the container and levelling the container are also done to achieve signal constancy during repeated tests.

The operator is required to wear a conductive strap connected to the table mat for safe operation of all ESD sensitive devices. LD current is monitored through a precise potentiometer and its optical output is monitored by the beam coming off the beam-sampler and going through a multimode beam pick-off fiber connected to a photodiode and/or oscilloscope.

4.2.2 Laser and Fluorescent Light Transmission through Illuminating and Receiving Fibers

Laser light illuminated from the LD is coupled through a straight-tip (i.e. ST) optical fiber connector into a fiber cable with a core diameter of 200 μm . After transmitting the light for about 1 m distance in the fiber, the fiber tip is housed inside a 1.1 mm diameter stainless steel distal tip. This illuminating tip touches a short-

pass filter which is mounted flush with the calibrating container's bottom surface and exposed to a doped FC-72 liquid film. Light yielded by fluorescence of the bi-acetyl in the solution is collected, after it is filtered by long-pass filters sitting flush on the fiber tip locations (R) on the probe surface, through six fiber cables mounted at offset locations (R) from the illuminating fiber cable (see Figures 2 and 3).

To improve the amount of fluorescent light collected through the receiving fibers, the doped solution is prepared at close to its highest allowable mass concentration, which is 0.20% dopant since the limit of bi-acetyl solubility in FC-72 at room temperature is found to be about 0.22% by mass. Clean, pure FC-72 solution is used throughout the tests to minimize the possibility of unwanted particles fluorescing under violet laser excitation. Operating temperature and current of the laser source are typically set, for various calibration and testing purposes, to be at 20°C and over a 40 to 60 mA range. Optical filters in all three sub-systems as indicated in Figure 6 are: one piece of 415 nm short-pass or SP (allows transmission of $\lambda \leq 415$ nm) at F1 (in the laser-to-fiber coupler) and I-fiber tips, one piece each of 470 nm long-pass or LP (allows transmission of $\lambda \geq 470$ nm) at the R-fiber tips and F2 (in the filter holder adaptor attached on the PMT), and additional 470-600 nm band pass filter and another 615 nm SP (allows transmission of $\lambda \leq 615$ nm) at F2. Spectral analysis is employed by using a spectrometer whenever the characteristics of noise light need to be ascertained towards improvement of signal-to-noise ratio or better understanding of the system.

Optimal offset distance, e , in Figure 3 for these tests is 1.7 mm. Total height of the optical testing container in Fig. 6 is 1" or 25.4 mm. However the top of this container also has a movable black disc, whose lower surface is initially at 6.6 mm from the bottom of the container. This movable disc can be lowered to effectively reduce the gap between the liquid-vapor interface and the top wall. As described later, it is this movable disc that allows a change between the configurations depicted in Fig. 9a and Fig. 9b.

During the tests, pure or doped solution is added into the calibrating container, which is designed such that a stationary and horizontal liquid film's thickness corresponds directly to the added liquid volume. At least two measurements are taken for each film thickness. Proper choice of the best signal scaling on the detector's oscilloscope helps in reducing the measurement errors. Values smaller than the oscilloscope ADC (analog-digital conversion) errors are discarded and the corresponding thickness/light levels determine the lower limits of the sensor's capabilities. All measurements need to be taken within one minute of laser illumination to prevent photo/thermal-degradation of the doped solution. LD degradation is also minimized by turning off the LD driver in between experimental runs.

Additional details of the calibrating container designed for the tests, experimental precautions, and procedures can be found in Ng [22].

4.2.3 Fluorescent Light Detection

Fluorescent light exiting the receiving fiber cable(s) is collimated by a collimating lens. The collimated light passes through a cylindrical barrel (1" inner diameter) which works as a filter holder adaptor. Inside the barrel, the light passes through some suitable optical filters and, finally, a suitable lens that focuses it on the active area of the photo-detector. During calibration or actual experimentation the photo-detector used is a

photomultiplier tube (PMT). However a spectrometer is used to replace the PMT during testing of the system components' and system's spectral response with the help of excitation light levels that are higher than what is used during actual dynamic film thickness measurements or calibration experiments. This testing allows detection and quantification of noise right outside of the desired fluorescent frequencies - providing both an understanding of the relative magnitude of noise light at these frequencies and a tool for optimizing the filtering of light at these frequencies, resulting in an improved signal-to-noise ratio in the actual experiments.

Sensitivity of the spectrometer can be adjusted for better detection and analysis of the optical spectrum. For cases when the PMT is used for actual calibrations and measurements, an oscilloscope is connected to the PMT with a coaxial cable. A resistor at the output end of the PMT converts the detected and amplified signals from amperes to voltage values before the signal reaches the oscilloscope. It should be noted that the rise times of PMT and spectrometer are 2.5 ns and 3 ms, respectively.

5. CALIBRATION EXPERIMENTS, PARAMETER DEFINITIONS, AND GOVERNING RELATIONSHIPS

5.1 Calibration Experiments

Calibration is performed by a paired set of experimental configurations (with and without liquid-vapor interface for a stationary horizontal liquid film) shown in Figures 9a and 9b below. The experiments are carried out with the help of the entire system indicated in Figure 6.

The purpose of a pair of calibration experiments for the same stationary and horizontal liquid film – first in the experimental configurations of Figures 9a followed by measurements in the experimental configuration of Fig. 9b - is to develop a calibration curve that fulfills the requirement of having achieved a certain one-to-one correspondence among various detected signals. To discuss this further, it is essential that these signals and issues associated with their measurements be defined first. This is done in the next section.

5.2 Important Definitions of Relevant Quantities

N_p (Unit: mV measured on the detector): Noise light (light other than the fluorescent light when either of the two configurations in Fig. 9 is used to provide the liquid film shown in the system of Fig. 6) that is received through receiving fibers R despite all the earlier described filtering at: inside the LD-to-fiber coupler, I-tip, R-tips, inside the filter holder adaptor in front of the detector, etc. This N_p is measured as amount of detected light – from the entire system (Figure 6) – when the liquid films used in the configuration shown in Figs. 9a or 9b is pure and there is no fluorescence. As needed, N_p for the experimental configuration of Figure 9a is denoted as N_{pIL-V} because of the presence of a liquid-vapor interface L-V and N_p for the experimental configuration of Figure 9b is denoted as $N_{pINo L-V}$ because of an absence of a liquid-vapor interface L-V. Unless otherwise stated, N_p denotes N_{pIL-V} . Ideally, if it was not for limitations imposed by the requirements underlying the principle of the sensor, technology, and cost; one would try to achieve $N_p \approx 0$ relative to the

signal of interest. In reality a non-zero value for N_p arises from the following sources: (i) some feeble noise light (that is predominantly in the fluorescent range of interest and is from the LD or auto fluorescence in the LD housing) that gets out of the I-tip, reflects off from the liquid-vapor interface and/or enclosure and enters the R-tip, (ii) some feeble noise light that gets generated by auto-fluorescence in the illuminating and receiving fibers' interaction with the illuminating light (typically the 408 nm excitation light), and (iii) some noise signal readings that arise from some inherent electrical noise in the electronics.

S_{fl-v} (Unit: mV measured on the detector): The fluorescent signal that is received through the receiving fibers when the liquid film is in the configuration of Figure 9a – a configuration in which the film has a liquid-vapor interface. This signal S_{fl-v} is due to: (i) direct collection (by the R-tips in Fig.2) of fluorescent light, from the primary illumination cone of Fig. 3, (ii) indirect reception of fluorescent light (also from primary illumination) at R-tips after its reflection from the liquid-vapor interface, and (iii) additional reception of fluorescent light at R-tips due to fluorescence in the secondary illumination zone (i.e. the *zone* formed by reflection of the illuminating light from the liquid-vapor interface, and/or other subsequent reflections between the solid-liquid interface and liquid-vapor interface; see Figure 3).

D (Unit: mV measured on the detector): Total detected light – from the entire system (see Figure 6) – for a doped film in the configuration of Fig. 9a or Fig. 9b. Ideally, for the configuration in Fig. 9a, one should have $D = S_{fl-v}$. However, because of a non-zero noise N_p , $D = S_{fl-v} + N_p$.

N_p/D (Unit: Dimensionless): Noise-to-detected light ratio (also called noise ratio). It is desirable that this ratio be made as small as possible. The smaller the value of N_p/D , the closer is the value of D to S_{fl-v} and the greater is the possibility of bringing it close to the desired signal $S_{flNo L-v}$ defined below.

$S_{flNo L-v}$ (Unit: mV measured on the detector): When the doped film is in the experimental configuration depicted in Figure 9b, the fluorescent signal, $S_{flNo L-v} \equiv D - N_p$, is computed from the measured values of D and N_p for this configuration. In this configuration, there is a complete absence of liquid-vapor interface as it is replaced by a liquid-solid (black surface) interface, and hence, there is a nearly complete absence of any reflection of light from the wetted top surface. Therefore $S_{flNo L-v}$ is the *measure* of the signal associated with direct collection of fluorescent light (light that directly goes to the R-tips) from the primary illumination zone. This is because the liquid-solid interface that replaces liquid-vapor interface absorbs almost all of the illuminating and fluorescent light reaching the solid black surface.

Other Terms and Definitions

- C** (Unit: %): Solution concentration = mass of dopant / mass of total solution * 100%.
- d** (Unit: mm): Local liquid film thickness (see Figure 9).

- e** (Unit: mm): Distance between the edges of illuminating and receiving fiber probes (see Figure 9).
- E_{LD}** (Unit: mA): Excitation light that transmits out of I-tip. It may contain some noise light. It is characterized by the current, in mA, that drives the laser in constant current mode near its zero output level (see Fig. 7c).
- I** Illuminating fiber.
- R** Receiving fibers.
- T** (Unit: °C): Temperature of liquid film.
- Θ** (Measured in degree): Local interface angle with respect to the horizontal (see Fig. 3 or Fig. 10). Clearly $\Theta = 0^\circ$ for a static horizontal interface. However $\Theta = \pm 3\text{-}20^\circ$ for many dynamic films of interest.
- BP** Band-pass filter, which allows transmission of light within specific wavelengths λ_1 and λ_2 .
- LD** Laser diode.
- LP** Long-pass filter, which allows transmission of light with wavelengths longer than a specific wavelength λ_L (i.e. $\lambda \geq \lambda_L$).
- SP** Short-pass filter, which allows transmission of light with wavelengths shorter than a specific wavelength λ_S (i.e. $\lambda \leq \lambda_S$).
- PMT** Photomultiplier tube.
- TEC** Thermoelectric cooler.

5.3 Governing Relationships Among Relevant Parameters and Factors

The following relationships highlight the principles underlying the calibration of the sensor through the film configurations recommended in Figures 9a to 9b. These relationships show the dependent factors associated with various signals collected by the sensor.

Equation 1: Experimentally Detected Light D for Doped Film and Factors Influencing It In The Configurations (Figs. 9a-9b) of Interest

$$\begin{aligned}
 D &= S_{\text{FIL-V}} \text{ (or } S_{\text{FILoL-V}}) + N_P & (1) \\
 &= \text{Function } (N_P, C, d, e, E_{LD}, T, \theta, \text{ etc.}^*) \\
 &= \text{Function } (N_P, d, \theta) \text{ if concentration } C \text{ and system settings are constant} \\
 &\approx \text{Function } (d) \text{ - if concentration } C \text{ and system settings are constant, and specially designed receiving} \\
 &\quad \text{fiber arrangement (Figure 2) and hardware improvements allow insensitivity of } D \text{ and } N_P \text{ values to} \\
 &\quad \text{changes in interface angle, } \theta.
 \end{aligned}$$

(* Examples of other factors (described more fully in section 7) are: photo-detector's area, type and number of optical filters in the system, opposite wall reflectivity, indices of refraction of the doped liquid and vapor, reflectivity and diffusivity of nearby surfaces, time duration of solution excitement by laser, ambient light (dark room, day, night, etc.), location and size of I and R fibers, etc. Also see "Other Terms and Definitions" in Section 5.2 for variables such as E_{LD} , T , etc.

Equation 2: Fluorescent Signal S_{fl-L-V} in the Presence of Reflected Fluorescent Light (due to primary illumination) from Liquid-Vapor Interface and Some Fluorescent Light from Secondary Illumination (see Fig. 3 and Fig. 9a)

$$S_{fl-L-V} = D - N_{PIL-V} \quad (2)$$

= Function (C, d, e, E_{LD} , T, θ , etc.*)

= Function (d, θ) - if concentration C and system settings are constant

\approx Function (d) - if concentration C and system settings are constant, and specially designed receiving fiber arrangement (Figure 2) and hardware improvement allow insensitivity to changes in interface angle θ .

Equation 3: True Fluorescent Signal $S_{flNoL-V}$ of interest in the Absence of Liquid-Vapor Interface (see Figure 9b arrangement that implies no reflected illuminating light and no reflected fluorescent light and hence no θ dependence)

$$S_{flNoL-V} = D - N_{PINoL-V} \quad (3)$$

= Function (C, d, e, E_{LD} , T, etc.*)

\approx Function (d) - if concentration C and system settings are constant.

6. RESULTS, CHALLENGES, ERRORS, AND SENSOR'S RESOLUTIONS

6.1 Challenges

There were three main challenges associated with the development of the proposed sensor. The challenges are related to the elimination of effects associated with the presence of noise light, elimination/containment of effects associated with the expected changes in liquid film's interface angle θ under conditions of a dynamic film, and reduction of errors by minimizing variations in the so called fixed system settings and hence improving repeatability of data at fixed levels of N_p and θ .

6.1.1 Noise Light Challenge

For both the configurations in Fig. 9, reduction in noise light N_p is very important. If N_p is not sufficiently small with respect to detected light D, it may not be possible to correlate the detected light D to the illuminated liquid film thickness that characterizes the volume of the primary illumination cone in Fig. 3. Under these high N_p/D conditions, the required one-to-one correspondence between D and the fluorescent signals S_{fl-L-V} and $S_{flNoL-V}$ typically either does not exist or the correspondence is unsatisfactory. As a result, for large N_p/D values, measurement of liquid thickness may not be possible over a range of thicknesses of interest. All these problems associated with large N_p/D are exemplified by a representative experimental result shown later in Figure 16 of this paper and in Figures 31 and 32 of Ng [22].

Even if, say on a detector, a noise light level of $N_p \approx 10^6$ times the illuminating light intensity is achieved through good filtering at various locations, the fluorescent signal $S_{\text{fil-V}}$ remains very small – typically only about 2-11 times N_p . This is because of the ultra-small level of fluorescent light $S_{\text{fil-V}}$ yielded by the ultra-small primary illumination (see Figure 3) in comparison to the level of noise light N_p associated with various noise sources in the system. As a result, there are practical limitations on significantly increasing signal-to-noise ratio ($S_{\text{filNo L-V}}/N_p$) or detected-light-to-noise ratio D/N_p . These practical limitations, despite the employment of state-of-the-art technology involving high quality optical filtering, photomultiplier tube detection (for very low level of light), high quality fiber-optic cables, and very high quality optics and electronics for the remaining system required development of a novel and effective calibration procedure. To address this problem, use of the proposed paired set of calibration experiments indicated in Figures 9a-9b led to a situation that does not require complete elimination of N_p or very significant enhancement of $S_{\text{fil-V}}/N_p$ or D/N_p values. The novel calibration technique developed here can be effective despite an unavoidable presence of a non-zero N_p provided it is within certain bounds (e.g. $S_{\text{fil-V}}/N_p$ is between 2-10 and the required one to one correspondence among D , $S_{\text{fil-V}}$, and $S_{\text{filNo L-V}}$ is achieved).

6.1.2 Interface Angle Challenge

In addition to the calibration with stationary films addressing challenges associated with noise light N_p , there is a need for local film thickness measurement even in the presence of waves. This requires development of a measurement approach that minimizes the dependence of detected signals D and $S_{\text{fil-V}}$ on the interface angle θ . The measurement principles are highlighted by Equations 1 and 2 of section 5.3. From there it is known that the θ dependence in the collected signal is largely due to the component of fluorescent and noise lights that are collected after their reflections from a potentially wavy interface. As long as the energy carrying wavelengths λ associated with typical interfacial waves can be assumed to satisfy, approximately, $\lambda > 8 \cdot a$ (where $a = 200 \mu\text{m}$ is the base diameter of the illuminating beam at the interface), the interface seen by the primary illumination cone can be modeled, for most waves of interest, as locally planar with different inclination angles θ (see Figure 10). The desired θ independence for D and $S_{\text{fil-V}}$ has been nearly achieved by a combination of two approaches.

The first approach is to use optimal location (distance e in Figure 2), optimal (which is minimal) laser excitation current, and optimal filter settings so as to reduce the reflected light component of $S_{\text{fil-V}}$ by minimizing $|S_{\text{fil-V}} - S_{\text{filNo L-V}}|$. That is, the first approach is to operate the calibration experiment in the actual configuration of Figure 9a such that this configuration's results are as close as possible to the results obtained from the associated calibration experiment in the desired ideal configuration of Figure 9b. The second approach consists of using an array of receiving fibers R (number ≥ 6) in the symmetrical arrangement shown in Figure 2. For $\theta = 0^\circ$, the illumination zone in Figure 3 is symmetric with respect to *any* line LL passing through the center of the illuminating fiber in the plane of the probe (see Figure 2). For two or three dimensional wave motions for which the interface can be approximated as *some* locally inclined plane of $\theta \neq 0^\circ$, there exists *some* instantaneous line LL in the plane of the probes as shown in Figure 2, with respect to

which the collected fluorescent light (directly or indirectly emanating from the primary and secondary illumination zones) has an anti-symmetric distribution. The total signal collected from the symmetrical arrangement of receiving fibers cancel signal increases over half of the receiving fibers on one side of LL with signal decreases over the remaining half of the receiving fibers on the other side of LL.

By a combination of the two approaches described above, suitable θ independence in the values of D has been experimentally verified for $-10^\circ \leq \theta \leq +10^\circ$ (see definition of θ in Figure 3). The resulting variations in D are within $\pm 5.0\%$ and because of the slope of the “ D vs d ” curve, these variations still lead to a good resolution of the film thickness, d , (± 0.09 mm for 0.5 mm $\leq d \leq 1.5$ mm and ± 0.18 mm for 1.5 mm $\leq d \leq 3.0$ mm) over the thickness range of interest.

For most wavy situations, one only needs θ independence over $-\theta_{\max} \leq \theta \leq \theta_{\max}$. The maximum interface angle $\theta = \theta_{\max}(d)$ in Figure 10 depends on the maximum amplitude a_w of the waves (assumed here to be less than 30% of film thickness d). Let the minimum wavelength λ_{\min} be such that, for $\lambda \geq \lambda_{\min}$, the wave energy in the dynamic film cannot be ignored. This gives, through Figure 10, a simple estimate of $\theta_{\max}(d) \approx \arctan(4a_w/\lambda_{\min})$. For 0.5 mm $\leq d \leq 3.0$ mm and typical FC-72 waves of $\lambda \geq \lambda_{\min} \approx 1$ cm, this gives a θ_{\max} of approximately 3° to 20° . This type of sensor’s range of applicability is determined by the experimentally determined value of $\theta_{\max}(d)$ for which θ independence can be confirmed. For a known $\theta_{\max}(d)$, the sensor can resolve, within certain bounds, instantaneous thickness for waves with minimum wavelength λ_{\min} (i.e. all $\lambda \geq \lambda_{\min}$) and maximum amplitude a_w provided the criterion

$$\lambda_{\min} > 8 \cdot a \quad (4)$$

for planar approximation of the interface, and the criterion

$$\arctan(4a_w/\lambda_{\min}) \leq \theta_{\max} \quad (5)$$

for staying within an experimentally verified zone of θ independence ($-\theta_{\max} \leq \theta \leq +\theta_{\max}$) is met. The experimental values of θ_{\max} were obtained by tilting the horizontal flat interface of Fig. 11a to other interface angles (to the extent possible by the available arrangements of the type indicated in Fig. 11b), which are $\theta = 0^\circ, 5^\circ, 10^\circ$, etc. to study the effect of θ on signal D while holding the mean value of film thickness d the same.

6.2 Calibration Results, Errors, and Sensor’s Resolution

6.2.1 Calibration Results

One of the three curves shown in Figure 12 gives the principal “ D vs. d ” calibration curve for a film that should remain valid even for dynamic films under environmental conditions similar to the one in Fig. 9a. The other curves in Figures 13-15 demonstrate the attainment of the required one-to-one correspondence between “ D vs. $S_{\text{FIL-V}}$,” “ $S_{\text{FIL-V}}$ vs. $S_{\text{FINO L-V}}$,” and “ $S_{\text{FINO L-V}}$ vs. d ” relationships. For cases with high D/N_p , such as the one in Fig. 16, “ D vs. $S_{\text{FIL-V}}$ ” fails to achieve one-to-one correspondence and the calibration principle is not satisfied. The reported results are from experiments for the paired set of calibration described in Section 5.1 for stationary horizontal films with interface angle of 0° . In fact the linearity of “ $S_{\text{FINO L-V}}$ vs. d ” curves, as shown in Fig.12 and Fig.15, is theoretically expected. Although, in principle, this straight line fit should pass through $S_{\text{FINO L-V}} = 0$ when $d = 0$; the experimental results show an offset not only in Figures 12 and 15, but

also in other experimental results (e.g. see Figures 64 to 67 of Ng [22]). This is, in all likelihood, due to some non-linear behavior over $0 \leq d \leq 0.5$ mm that arises from the fact that for very small d values, for which e/d (e is offset in Figure 3) is large, the receiving fibers have stopped receiving light that is dominated by *direct* fluorescent light from the primary illumination cone of Fig. 3. The nature of this part of the curve – which represents small detected light (closer to the noise light levels) that arrives at the R-tips of the receiving fibers *indirectly* (i.e. after its reflection from the interface) - is not experimentally determined but is schematically shown in Figure 15 as a dashed curve OO’.

The one-to-one correspondence obtained in Figs. 13-15 establish the functionality of the proposed calibration principle which allows use of this sensor without requiring $N_p \approx 0$ or $D \approx S_{\text{FINo L-V}}$. All that is required is that the departure amounts of $N_p \neq 0$ and $D - S_{\text{FINo L-V}} \neq 0$ must be such that the one-to-one correspondence of the types shown in Figure 13 to 15 be achievable.

Once the in-situ calibration curve of “D vs. d” of the type shown in Fig. 12 is available and it satisfies the one-to-one correspondence principle of the type shown in Figures 13 to 15, one can use the calibration curve of Fig. 12 to convert experimentally measured values of time-varying signal D - in an actual sensor application involving a dynamic film (in a configuration similar to the one described by Fig. 9a) - to obtain the corresponding time varying values of film thickness d . The time varying values simply follow from associating the instantaneous values of signal D with instantaneous thickness d - through the type of “D vs. d” curve shown in Figure 12.

6.2.2 Errors and Resolution

The developed sensor has errors in the detected light D and these calibration errors need to be related to the error or resolution in the measurement of film thickness d . The errors are of types E_1 , E_2 , and E_3 described below.

E_1

E_1 are errors associated with the fact that experimentally detected light D does not achieve perfect θ independence.

In real applications of the developed sensor, to find the film thickness d , a calibrated “ $S_{\text{FINo L-V}}$ vs. d ” curve should ideally be used instead of the experimentally obtained “D vs. d ” curve. However using the experimentally obtained D values alone is practical because experimental measurements only give the D signals and any use of the underlying calibration curves must come from the pair of separately performed calibration experiments. Errors E_1 associated with the measurements in D are the variations of D due to changes in θ . A maximum errors of $E_1 = \pm 5.0\%$ times D was achieved for the reported results (for $\theta_{\text{Max}} = 10^\circ$) and these are shown as vertical bars in “D vs. d ” curve of Figure 12. The reported errors E_1 have been obtained from calibration experiments performed for $\theta = 0^\circ$ and various angles up to $\theta_{\text{Max}} = 10^\circ$.

It is expected, when hardware changes to facilitate experiments over $-20^\circ \leq \theta \leq 20^\circ$ becomes available, θ independence over a much larger range will be experimentally verified. Even for waves with θ in the larger range, the sensor’s resolution can be further improved without sacrificing its range of applicability as far as its

ability to resolve instantaneous film thickness are concerned. For example, if it is found that, for a larger θ_{Max} , E_1 can only be contained within $\pm 7\text{-}9\%$ of D , then the sensor's resolution (see definition in eq. 6 below) can still be further improved because increasing the number of symmetrically placed receiving fibers in Figure 2 improves resolution by increasing $\partial D/\partial d$ values (more ΔD for same Δd) in eq. (6) below.

E_2

E_2 are errors due to variations in concentration and temperature of doped solution from those at reference concentration and reference temperature employed in obtaining the temperature curves. This type of error can be minimized by picking the most suitable reference concentration and reference temperature.

If one's concentration of interest is in the range of $0.15\% \leq C \leq 0.20\%$ and temperature of interest is in the range of $20^\circ\text{C} \leq T \leq 40^\circ\text{C}$, one can use other calibration curves of the type shown in Figures 17 to 18 (also see Ng [22]) to obtain an interpolated curve of "D vs. d" at the concentration C and temperature T of interest. Use of such interpolated curve or curves will lead to minimal errors E_2 (say $< 0.2\%$) because the interpolated curve will correspond to a new set of reference concentration and reference temperature that is close to the concentration and temperature of interest. Therefore, for the present calibration purposes, errors E_2 are not considered to be part of the total error E_T that should be used to define the sensor's resolution.

E_3

E_3 are errors associated with imperfect variations in fixed system settings (e.g. rigidity of optical connectors, quality of temperature and current control of laser light source, resolutions of various electronic instruments, etc.). These errors have been found, through repetition of experiments for the reported data set, to be within $\pm 1.1\%$ of D .

E_T

Total error E_T associated with the detected light D from the developed sensor is computed from: $E_T = [E_1^2 + E_2^2 + E_3^2]^{1/2}$. This definition of E_T is valid, as long as the underlying assumptions of causal independence among E_1 , E_2 , and E_3 and the assumption of Gaussian distribution of each of the error components (if sufficient and large number of experiments were performed) are considered to be reasonable.

Due to variations in E_1 with film thickness, each film thickness value has, in general, different E_T associated with its D . Over the entire range of $0.5 \text{ mm} \leq d \leq 3 \text{ mm}$, E_T is calculated to be within $\pm 5.1\%$ of D . E_T for $S_{\text{fil-V}}$ and $S_{\text{filNoL-V}}$ are similarly obtained through the indicated use of associated error bars in Figures 13 to 14 (see ab , $a'b'$, and $a'b''$). In any graph, the horizontal error bar (e.g. $a'b'$ in Figure 13) is obtained by dividing the associated vertical error bar (ab) by the mean local slope of the curve in the figure (i.e. "D vs. $S_{\text{fil-V}}$ " curve's slope in Figure 13).

Sensor Resolution

The sensor's resolution at any measured film thickness d is given by

$$\Delta d \cong \left\{ 1 / \frac{\partial D}{\partial d} \right\} \cdot E_T \quad (6)$$

where E_T is the total error and $\partial D/\partial d$ is the slope of the “D vs. d” calibration curve in Fig. 12. The overall resolution Δd_o of the sensor is defined to be the maximum of Δd values obtained, over a range of d values, from eq. (6).

7. SUMMARY OF ACTIONS TAKEN TO ENSURE THAT ONLY THE DETECTED LIGHT (D) AND THE COMPUTED VALUES OF $S_{fil-L-V}$ AND $S_{fil-No L-V}$ CHANGE AS FILM THICKNESS d CHANGES

As in any measurement system, a direct correlation is desired between the detected light (D), which is received by the measurement system, and the film thickness (d), which is the physical parameter of interest. It is, therefore, desirable to eliminate any other factors which affect the detected light level or keep their contribution to a known, narrowly defined level. In this section, some of the additional parameters contained in our measurement system which influence the detected light will be summarized, along with the efforts taken to make them constant (and known through the paired calibration experiments and other noise light analysis) or eliminate them.

7.1 Reduction of Noise Light, N_p

As discussed in Section 6.1.1, there is noise light which arises from fluorescence of reflected excitation light or reflection of fluoresced light from the liquid–vapor interface in the secondary illumination cone of Figure 3. Additionally, this noise light may arise from a number of other sources, such as the fibers, collimators, connectors, and interfaces the light crosses or contacts within the system. Our methods of reducing or controlling this noise light are listed briefly below.

- Filters in Laser Housing
 - o Filters have been installed in the laser housing to prevent unwanted long wavelength light (near or in the frequency band of the detected fluorescent light) from being released from the laser diode into the illuminating fiber.
- Filters at Tip of Illuminating Fibre
 - o At the tip of the illuminating fiber, a short pass filter has also been installed to prevent long wavelength light (> 415 nm) not blocked by the laser housing filters or resulting from auto fluorescence in the illuminating fiber and associated fittings (ST connector and collimators) from entering the film. Such light may pass the receiving fiber filters and get detected in D.
- Special Aluminium Calibration Chamber
 - o An aluminium calibration chamber with a black, anodized surface and cover was constructed to reduce the reflection of illuminating and fluorescent light, restricting most of the light to the primary or secondary illumination cones of Figure 3. Additionally, this chamber was designed to reduce ambient light entering it which might interfere with the operation of the sensor by introducing additional light in the excitation and /or fluorescent wavelength ranges.
- Filters at Tips of Receiving Fibers

- Filters were also placed at the tips of the receiving fibres to block non-fluorescent light (< 470 nm) from being detected. They block illuminating light and high frequency noise light from other sources from entering the receiving fibers.
- Filters between Receiving Fiber Connector (SMA 905) and Photodiode or Photomultiplier Tube
 - Between the receiving fibres and the sensing device, additional optical filters have been installed to reduce auto fluorescent or illuminating light from receiving fibers which enters the sensing device, along with all other noise range outside the 470 – 600 nm region of interest.
- Photomultiplier Tube for Detection, Coupled with a Very Low Excitation Light Level
 - Because of the high sensitivity of the photomultiplier tube to light (3000 times more sensitive than a typical photodiode [22]), much lower levels of excitation light may be used, while still yielding a sufficient level of detected light for resolving film thickness. The main advantage of a low level of illuminating light is that it reduces the reflection of illuminating and fluorescent light from the liquid–vapour interface or liquid–surface interfaces. Additionally, it reduces auto fluorescence in the physical light path from instrumentation and hardware.

7.2 Control Over the Concentration of Dopant (C) and the Level of the Illuminating Light (E_{LD})

- Doped Solution Prepared with Precise, Electronic Mass Scale and Syringe
 - By measuring carefully the mass of FC-72 and dopant on a mass scale and adding the dopant with a syringe, it is easy to know and control the concentration of the doped solution in a repeatable manner, which we verify through absorbance measurements with the help of a dipping probe spectrometer for diagnostic and control purposes.
- Dopant Refrigerated when Not in Use
 - Refrigerating the bi-acetyl when not in use inhibits its natural degradation, preserving its optical properties as long as possible.
- Doped FC-72 Stored in Sealed Container
 - By sealing the doped solution of FC-72 and bi-acetyl, slight changes in concentration resulting from evaporative losses to the air are avoided.
- Illuminating Light Intensity Monitored with a Beam Splitter and Photodiode
 - To assure that the light output remains the same between calibrations and data acquisition, the intensity of the illuminating light is monitored using a photodiode which measures a portion of the illuminating light released through a beam splitter. The laser diode current is adjusted to maintain the desired light output using a current controlled power supply with an adjustable potentiometer. This provides repeatability for the illuminating light and allows for slow starting and shutting down of the laser diode, lengthening its usable life.
- Thermoelectric Temperature Control for Laser Diode

- As mentioned in Section 4.2.1, a thermoelectric system is utilized to control the temperature of the laser diode and its housing. This aids in the repeatability and stability of the light output from the laser diode.
- ST (“straight terminus”) Connector on Laser Diode Housing for Illuminating Fibre
 - After the laser diode housing filters, beam splitter, and collimator, the focused laser light enters the illuminating fiber through an ST connector. This connector was chosen because of its mechanical rigidity, minimizing losses while maximizing the repeatability and stability of the excitation light transmitted into the illuminating fiber.

7.3 Setting the Fiber Spacing (e), Fixing the Temperature (T), and Minimizing Interface Angle (θ) Effects

- Precise Holes Machined for Fiber Distal Tips
 - Holes for fiber distal tips were drilled in the calibration chamber at precise locations, one in the middle for the illuminating fibre, and 6 (or 1 for preliminary tests) annular holes for the receiving fibres, spaced (symmetrically for the case of 6 fibers) at 2 mm centre-to- centre distance from the illuminating fiber. This yields an “e” value of 1.7 mm, as shown in Figure 2, for 200 μm illuminating fibre and 800 μm receiving fibres. The distal tips allow the fibres to be removed for maintenance or to switch to a different calibration chamber or device containing the liquid film whose thickness is to be measured.
- Calibration Experiments Conducted at Ambient Room Temperature
 - The ambient temperature in the dark room was approximately constant and all experiments were carried out at ambient temperature.
- Doped FC-72 Stored at Ambient Room Temperature
 - To prevent the effects of varying liquid temperature with time, all doped FC-72 used in the calibration experiments was stored at room temperature before use.
- Symmetric Arrangement of Receiving Fibres
 - Due to the symmetric arrangement of the receiving fibres, anti-symmetry is averaged out of detected light and fluorescent signals, leading to a cancellation of most of the interface angle effects (covered in more detail in Section 6.1.2).

8. CAPABILITY VERIFICATION OF THE CALIBRATED SENSOR

The developed sensor has been used in a proof-of-concept experiment that has a time-varying film thickness at the measurement location.

Under forced (0 to 2 Hz) horizontal oscillations of the container (see [22] to note that the container and a lowered top disc together form a cylindrical hollow space of 2” diameter and height of 6.6 mm) in Fig. 19, local thickness measurements at an off-center location were performed. The oscillations caused the initially horizontal liquid film of thickness 1.5 mm to become dynamic – yielding a dynamic film of time varying thickness at the offset location (see, in Figure 19, the suggested but simplified interface configurations at

different times) where the film thickness is measured by the newly invented sensor. Note that the thickness oscillations at any point is not expected to be sinusoidal for two reasons: (i) somewhat non-sinusoidal nature of the forced oscillations, and (ii) sloshing – i.e. the long term nature of the waves being detected result from a superposition of the forced waves and its continuous reflections off the container’s walls.

The horizontal vibration ranging from 0 to 2 Hz was applied to the container by Accel Shaker from Labworks Inc. The film thickness measurements were found by signals D collected through the sensor. Under identical forcing conditions, independent film thickness measurements were also obtained by a direct mechanical measurement technique for the wave’s amplitude and the wave’s principal frequency (which was assumed to be the same as the shaker frequency). The separate and independent mechanical measurements were obtained at the same off-center location where the I-tip (Fig.2) of the sensor was in the experiment employing the sensor. The maximum wave amplitude was measured by placing a thin vertical needle directly above the off-center measuring location and by measuring the distance between the initial (prior to shaking) and final wetted lengths. The measurements yielded the amplitude of the oscillations whereas the time period $T (= 1/f)$ of oscillations was determined by the shaker’s frequency of 1 Hz.

The frequency and amplitude of the film thickness, as obtained by the newly invented sensor, are shown in Figures 20c and 20d. These measurements agree very well with independent measurements (marked by “x” in Figures 20c and 20d) of the time-varying film thickness’s amplitude and period of oscillations. This establishes that the sensor is able to resolve both the amplitude and the frequency of the dynamic film. More sophisticated comparison experiments (not available at this time) are in progress and they are likely to show very good agreement at all intermediate times – times between the crests and troughs – as well. The electronic and other noises of frequency greater than 10 Hz were filtered out for signal D, reported for dynamic films in Figures 20a and reported for static films in Fig.20b. The filtered signals are believed to more accurately represent the actual waves for this validation experiment.

9. FUTURE DIRECTIONS AND RECOMMENDATIONS

The sensor is undergoing better packaging and improvements so it can be used for real time thickness measurements in ongoing experiments that involve flow of adiabatic and condensing films on the bottom wall of a rectangular cross-section duct. Improvements will address the following: better packaging of the sensor probe and integration of optical filters on the sensor probe; improved resolution over a larger range of interfacial angles determined by θ_{Max} ; minimization of auto-fluorescence in optical fibers; in-situ calibration strategies in a duct which provides for rigid and repeatable optical connections, a light free interior, and clean interior walls that behave like a black-surface under minuscule excitation from the illuminating light source.

10. CONCLUSIONS

- Development and calibration of a fluorescence and fiber-optics based real-time film thickness sensor have been completed. The verified and developed measurement principle and the calibration experiments are of general value and can be used for fabricating any other sensor on this principle. Results for the

sensor developed here show that the detected light D and fluorescent light $S_{\text{fil-L-V}}$ increase with increasing liquid film thickness over a measurable range of 0.5 to 3.0 mm.

- Proposed calibration strategy is able to extract relevant information from experiments that show the presence of an unavoidable, non-zero amount of noise light N_P . This N_P is mostly due to presence of noise light in the illuminating light and due to optical components' auto-fluorescence under excitation from the illuminating light. Signal improvement tests, noise source analyses, and hardware modifications have been implemented that ensure extraction, from D , the relevant signal, $S_{\text{filNoL-V}}$, associated with fluorescent light under minimized presence of noise light, N_P , and minimized sensitivity of $S_{\text{fil-L-V}}$ to the inclination θ of the liquid-vapor interface.
- Developed sensor reaches a near θ independence for D and N_P by a combination of two approaches. The first approach is to use optimal location of fiber mounting, optimal laser excitation current, and optimal filter settings to reduce the reflected light component of $S_{\text{fil-L-V}}$ by minimizing $|S_{\text{fil-L-V}} - S_{\text{filNoL-V}}|$. The second approach is to use an array of six or more receiving fibers in a symmetrical arrangement surrounding an illuminating fiber.
- Effects of doped solution's concentration and temperature on signal D have also been investigated. Results show that D decreases when the concentration reduces from 0.20% to 0.15% and when the temperature increases from 20°C to 40°C. Such calibrations can be performed for other suitable ranges of concentration and temperature.
- After taking into consideration issues related to repeatability of experimental data, errors of +/- 1.1% of D were found to be a good estimate. The total error, E_T , associated with measurements of D can be minimized to within +/-5.1%. This leads to a reasonable film thickness resolution of +/- 0.09 mm (over 0.5 to 1.5 mm) and +/- 0.18 mm (over 1.5 to 3.0 mm).
- The developed sensor has also been used in a proof-of-concept experiment that has a time-varying film thickness at the measurement location. The frequency and amplitude measurements of the film thickness obtained by the sensor agree very well with independent measurements of amplitude and frequency of the time-varying film thickness.

ACKNOWLEDGMENT

This work was supported by the grants: NSF CTS-0086988 and NASA NNC04GB52G. We thank Dr. A.E. Smart [19] for his initial guidance at the beginning of this project. We also thank Ralph Swafford and Oz Optics, Canada for their advice and effort in making most of the custom optical components.

REFERENCES

- [1] Kumar, R., Gottmann, M., and Sridhar, K. R., 2002, "Film Thickness and Wave Velocity Measurements in a Vertical Duct," *Journal of Fluids Engineering*, **124**, pp. 634-642.

- [2] Tihon, J., 2004, "Hydrodynamics of the Solitary Waves Travelling Down a Liquid Film," *XXI International Congress of Theoretical and Applied Mechanics, August 15-21, 2004, Warsaw, Poland*.
- [3] Lu, Q., 1992, "An Experimental Investigation of Heat Transfer with Condensation in a Horizontal Rectangular Duct," *PhD Dissertation, MEEM Department, Michigan Technological University*.
- [4] Zaitsev, D. V., Kabov, O. A., and Evseev, A. R., 2003, "Measurement of Locally Heated Liquid Film Thickness by a Double-Fiber Optical Probe," *Experiments in Fluids*, **34**, pp. 748-754.
- [5] Shedd, T. A., and Newell, T. A., 2004, "Characteristics of the Liquid Film and Pressure Drop in Horizontal, Annular, Two-Phase Flow Through Round, Square and Triangular Tubes," *Journal of Fluids Engineering*, **126**, pp. 807-817.
- [6] Than, C. F., Tee, K. C., Low, K. S., and Tso, C. P., 1993, "Optical Measurement of Slope, Thickness and Velocity in Liquid Film Flow," *Smart Materials and Structures*, **2**, pp. 13-21.
- [7] Shedd, T. A., and Newell, T. A., 1998, "Automated Optical Liquid Film Thickness Measurement Method," *Review of Scientific Instruments*, **69**(12), pp. 4205-4213.
- [8] Qiu, H., Wang, X., and Hong, F., 2005, "Measurements of Interfacial Film Thickness for Immiscible Liquid-Liquid Slug/Droplet Flows," *Measurement Science and Technology*, **16**, pp. 1374-1380.
- [9] Wang, X., and Qiu, H., 2005, "Fringe Probing of Liquid Film Thickness of a Plug Bubble in A Micropipe," *Measurement Science and Technology*, **16**, pp. 594-600.
- [10] Nozhat, W. M., 1997, "Measurement of Liquid-Film Thickness by Laser Interferometry," *Applied Optics*, **36**(30), pp. 7864-7869.
- [11] Liu, A., Wayner Jr., P. C., and Plawsky, J. L., 1994, "Image Scanning Ellipsometry for Measuring the Transient, Film Thickness Profiles of Draining Liquids", *Physics of Fluids*, **6**(6), pp. 1963-1971.
- [12] Jones, G., Markvart, T., and Greef, R., 2001, "Deposition and Characterisation of Sensitising Dye Layers," *Post Graduate Conference in Engineering Materials Proceedings, 2001, University of Southampton, Southampton, UK*.
- [13] Wu, X. L., Levine, R., Rutgers, M., Kellay, H., and Goldburg, W. I., 2001, "Infrared Technique for Measuring Thickness of a Flowing Soap Film," *Review of Scientific Instruments*, **72**(5), pp. 2467-2471.
- [14] Mouza, A. A., Vlachos, N. A., Paras, S. V., and Karabelas, A. J., 2000, "Measurement of Liquid Film Thickness Using a Laser Light Absorption Method," *Experiments in Fluids*, **28**, pp. 355-359.
- [15] Giroud-Garapon, S., Heid, G., and Lavergne, G., 2003, "Thin Wall Liquid Film Thickness Measurement: A Video Optical Technique," *Proceedings of PSFVIP-4, June 3-5, 2003, Chamonix, France*.
- [16] Cho, H., and Min, K., 2003, "Measurement of Liquid Fuel Film Distribution on the Cylinder Liner of a Spark Ignition Engine Using the Laser-Induced Fluorescence Technique," *Measurement Science and Technology*, **14**(7), pp. 975-982.
- [17] Jeremy, M. C., Noel, T., and Doherty, W. G., 2004, "Laser Induced Fluorescence Measurements of the Thickness of Fuel Films on the Combustion Chamber Surface of a Gasoline SI Engine," *12th International Symposium, The Calouste Gulbenkian Foundation, July 12-15, 2004, Lisbon, Portugal*.
- [18] Hidrovo, C. H., and Hart, D. P., 2001, "Emission Reabsorption Laser Induced Fluorescence Film

- Thickness Measurement,” *Measurement Science and Technology*, **12**, pp. 467-477.
- [19] Smart, A. E., and Ford, R. A. J., 1974, “Measurement of Thin Liquid Films by a Fluorescence Technique,” *Wear*, **29**, pp. 41-47.
- [20] Hentschel, W., Grote, A., and Langer, O., 1997, “Measurement of Wall Film Thickness in the Intake Manifold of a Standard Production SI Engine by a Spectroscopic Technique,” *Society of Automotive Engineers*, Paper 972832.
- [21] Alekseenko, S. V., 1994, *Wave Flow of Liquid Films*, Begell House, New York.
- [22] Ng, T. W., 2006, “Development and Calibration of a Fluorescence and Fiber-Optics Based Real-Time Thickness Sensor for Dynamic Liquid Films,” *PhD Dissertation, MEEM Department, Michigan Technological University*.

LIST OF FIGURE CAPTIONS

- Figure 1:** Operating principle of a fluorescence sensor.
- Figure 2:** Symmetrical arrangement of R probes around an I probe.
- Figure 3:** Details of the neighborhood of illuminating (I) and receiving (R) fiber tips.
- Figure 4:** Absorbance spectrum of a bi-acetyl doped FC-72 solution ($C = 0.121\%$).
- Figure 5:** Fluorescent intensity versus wavelength curves (dashed line) of a bi-acetyl doped FC-72 solution for an excitation light of $\lambda = 425$ nm and concentration of 0.054% . The scaling factor curve (solid line) is proportional to the absorbance.
- Figure 6:** Schematic of the experimental setting for the developed sensor.
- Figure 7a:** Intensity scale: linear.
- Figure 7b:** Intensity scale: logarithmic.
- Figure 7c:** Operating specifications of Nichia NDHV310APCE1 violet LD.
- Figure 8:** Physical assemblies of a liquid film thickness sensing system.
- Figure 9:** Calibration experimental configurations (with and without liquid-vapor interface) and associated nomenclature.
- Figure 10:** Relationship of interfacial wavelength λ to the illuminating beam’s diameter at the interface.
- Figure 11:** Interface angle test.
- Figure 12:** Variations of D , S_{FIL-V} and $S_{FINO L-V}$ with film thickness d . The vertical error bars for D include errors E_1 due to variations in the interface angle within $\pm 10^\circ$ range. After obtaining D and N_p for both the configurations in Figure 9, S_{FIL-V} and $S_{FINO L-V}$ were respectively obtained from equations (2) and (3).
- Figure 13:** Correspondence of estimated error E_T for D and error for S_{FIL-V} .
- Figure 14:** Correspondence of estimated errors between S_{FIL-V} and $S_{FINO L-V}$ for this calibration
- Figure 15:** Resolutions Δd for the developed sensor.
- Figure 16:** Appearance of a non monotonic $D - S_{FIL-V}$ curve if N_p is not sufficiently small with respect to D .
This test was done under conditions of a higher LD excitation current.
- Figure 17:** Concentration effect on signal D at temperature of 20°C .

Figure 18: Temperature effect on signal D at concentration of 0.20%.

Figure 19: Dynamic liquid film measurement test that yields time-varying thicknesses.

Figure 20: Signal D obtained for dynamic and stationary films are shown in (a) and (b). The negative signal for D is due to switched polarity; the magnitude of this D corresponds to the value of D in the calibration curve of Fig. 12. Dynamic and stationary film thicknesses measured by the developed sensor at a fixed location and its comparisons with alternative measurements (marked x) are respectively shown in (c) and (d).

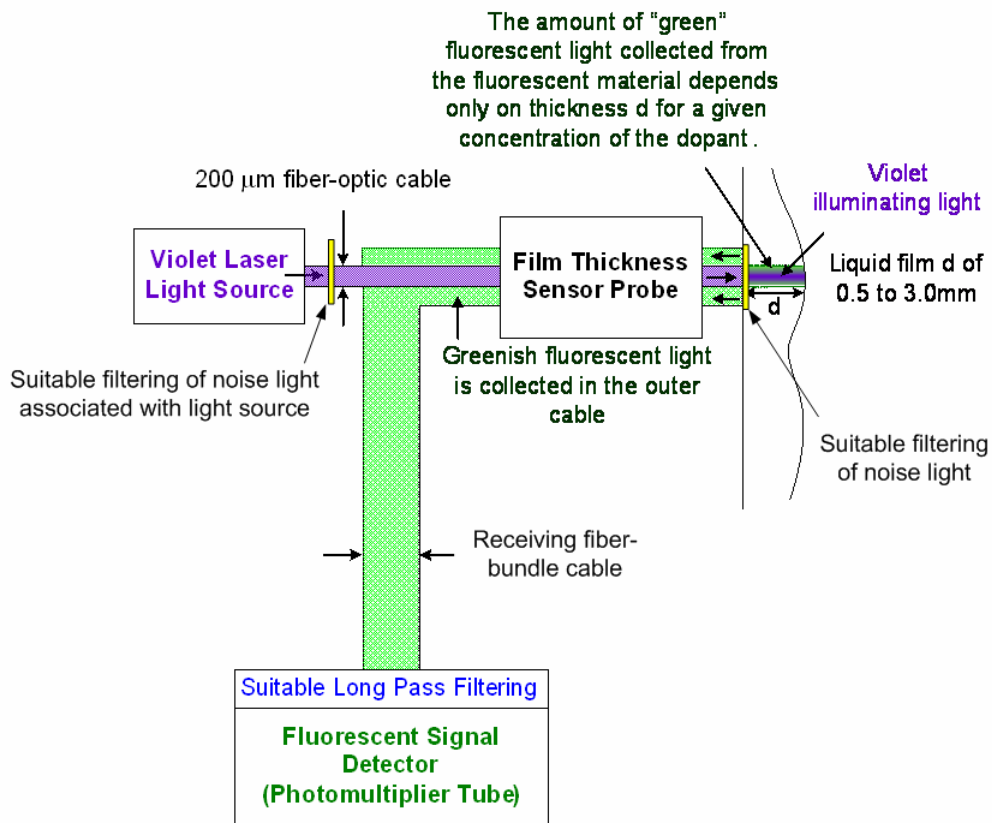


Figure 1

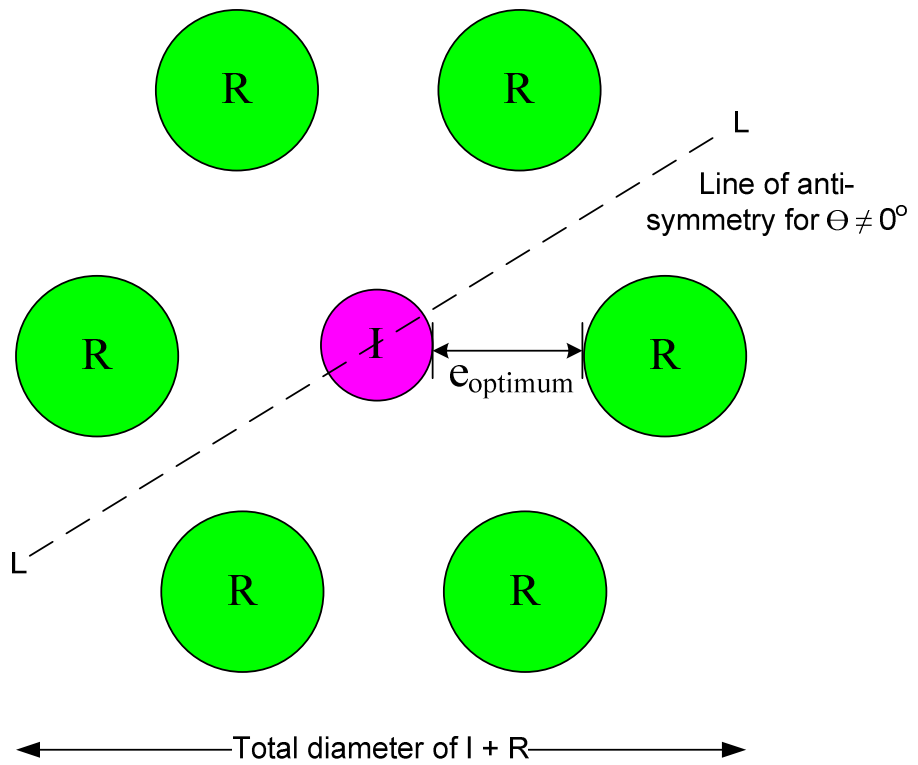


Figure 2

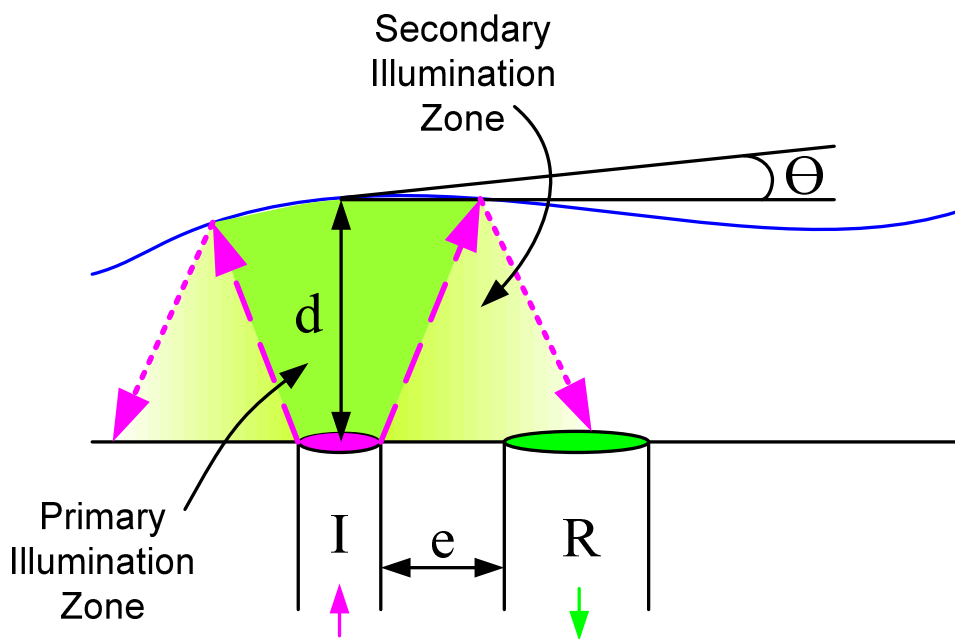


Figure 3

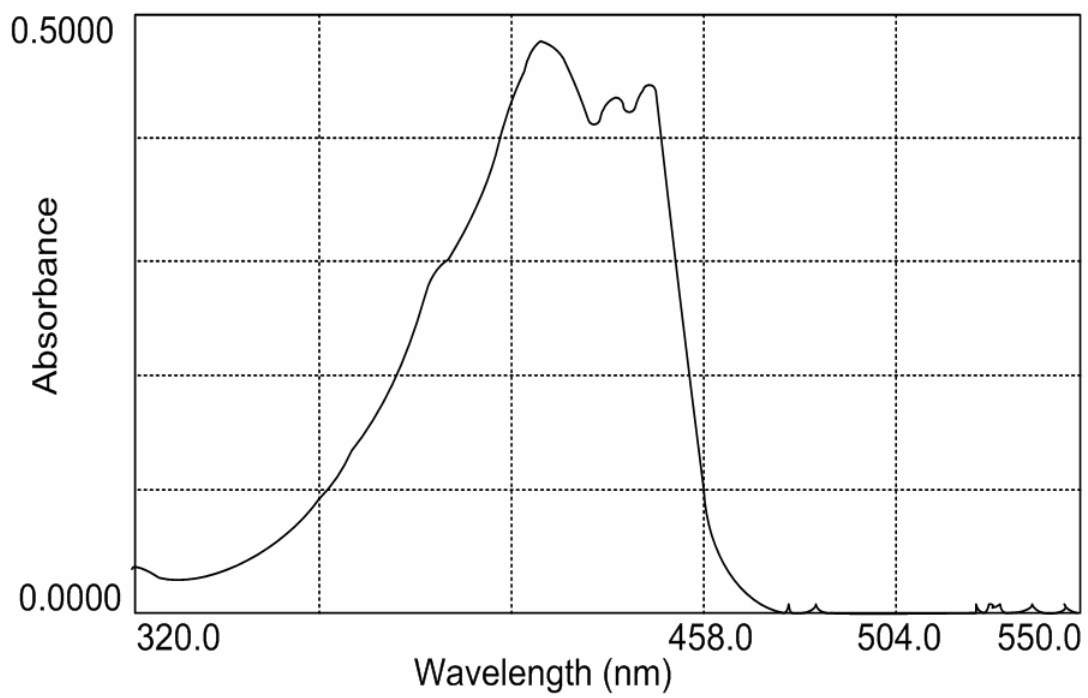


Figure 4

Doped FC-72 with concentration of 0.054 %

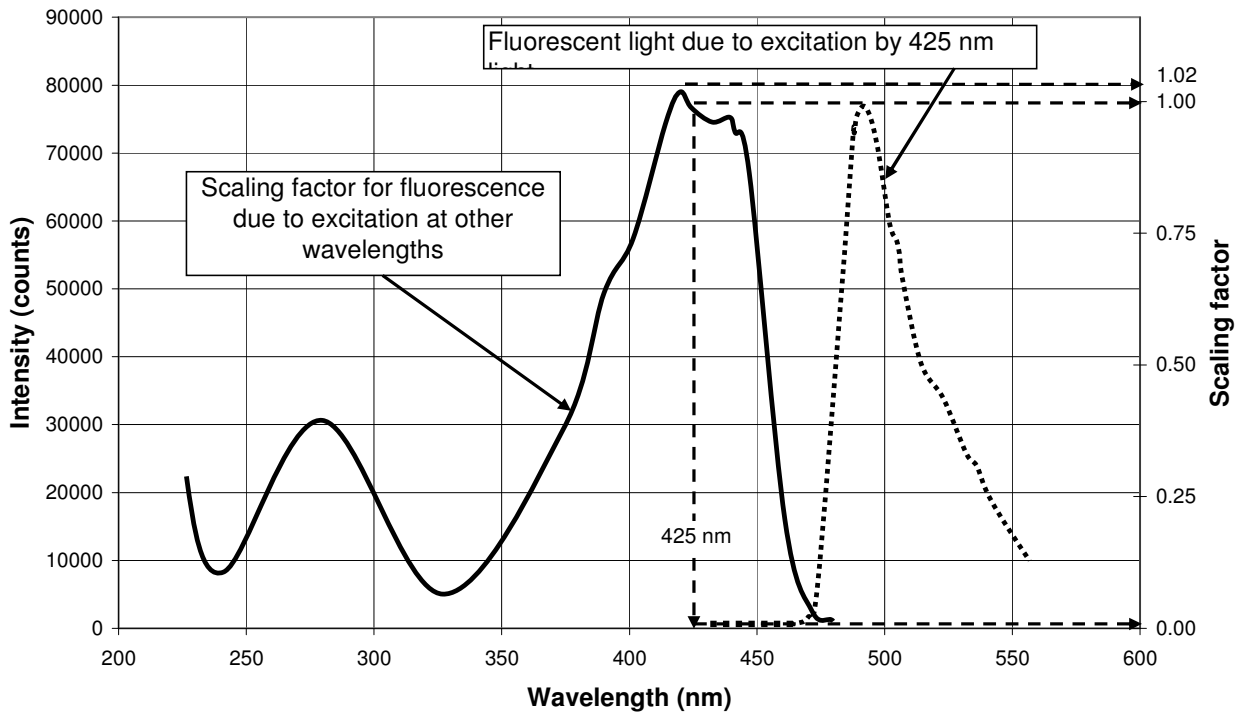


Figure 5

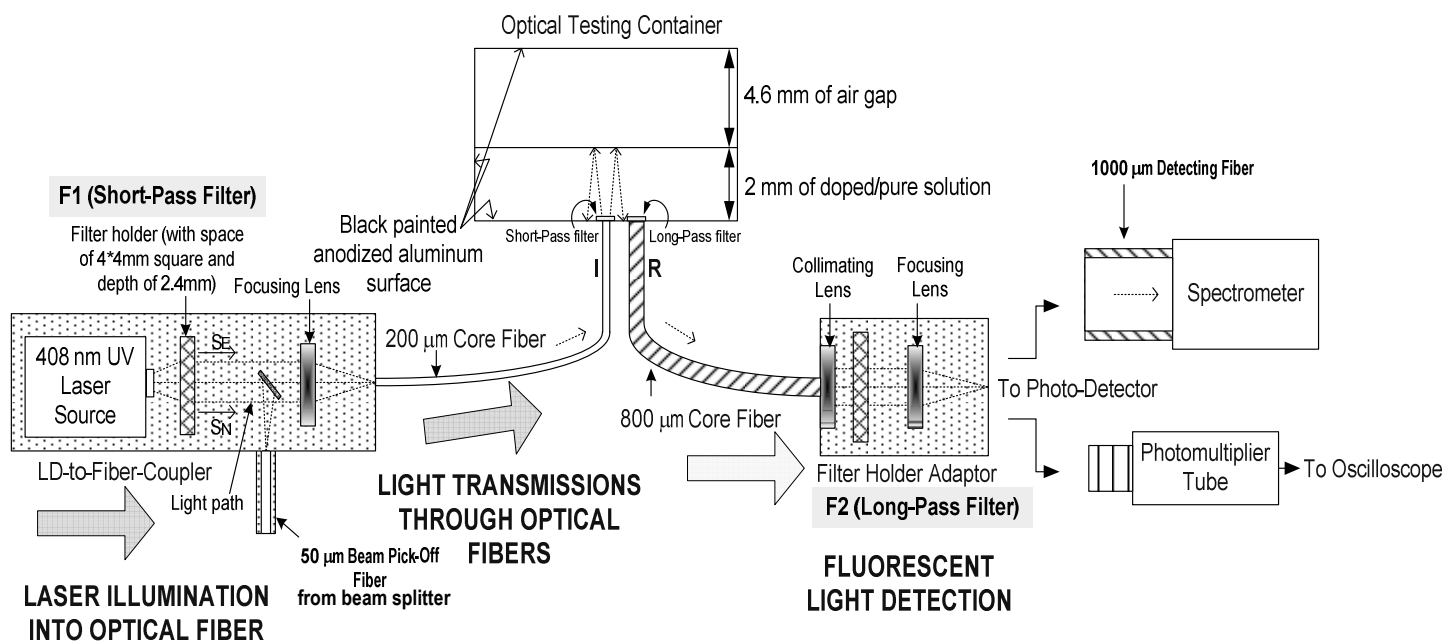


Figure 6

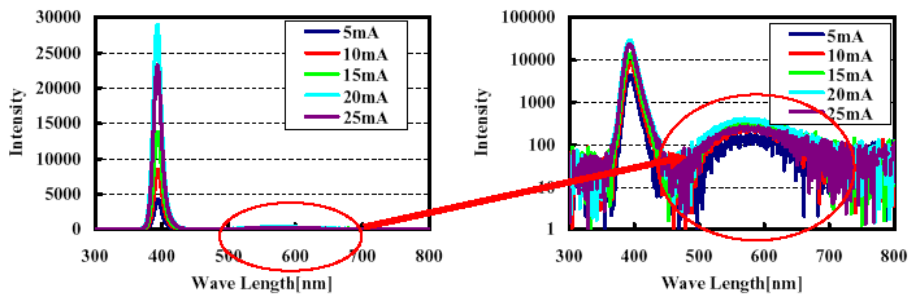


Figure 7a

Figure 7b

◆ Optical Output Power vs. Forward Current

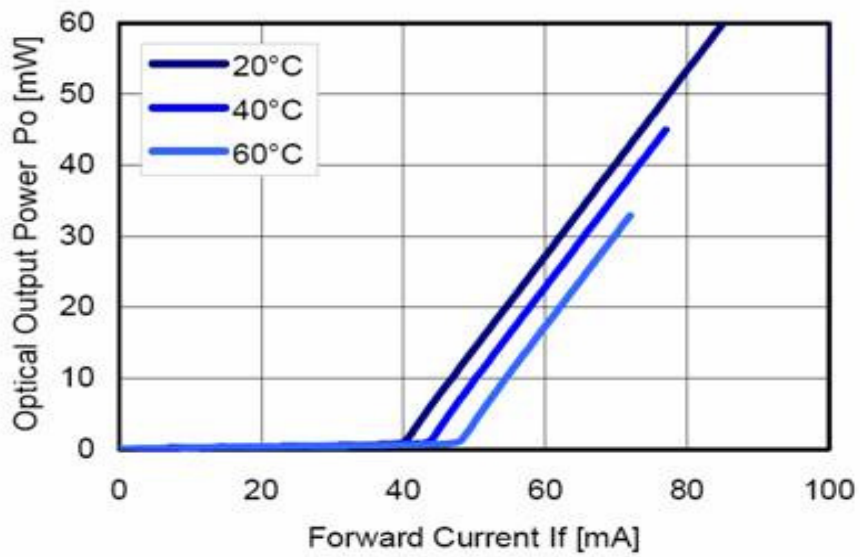


Figure 7c

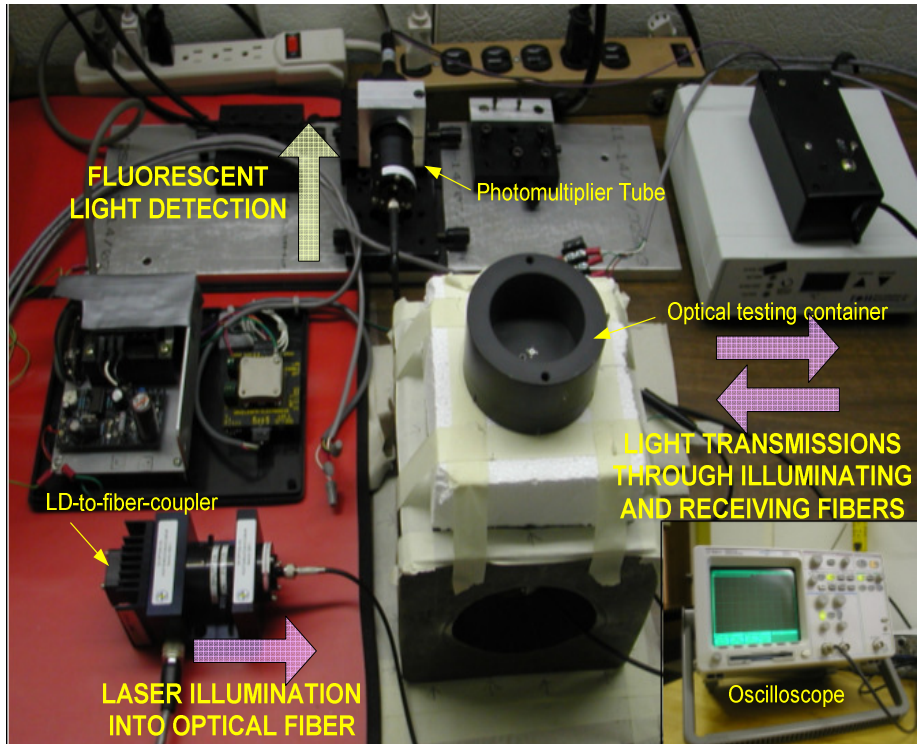


Figure 8

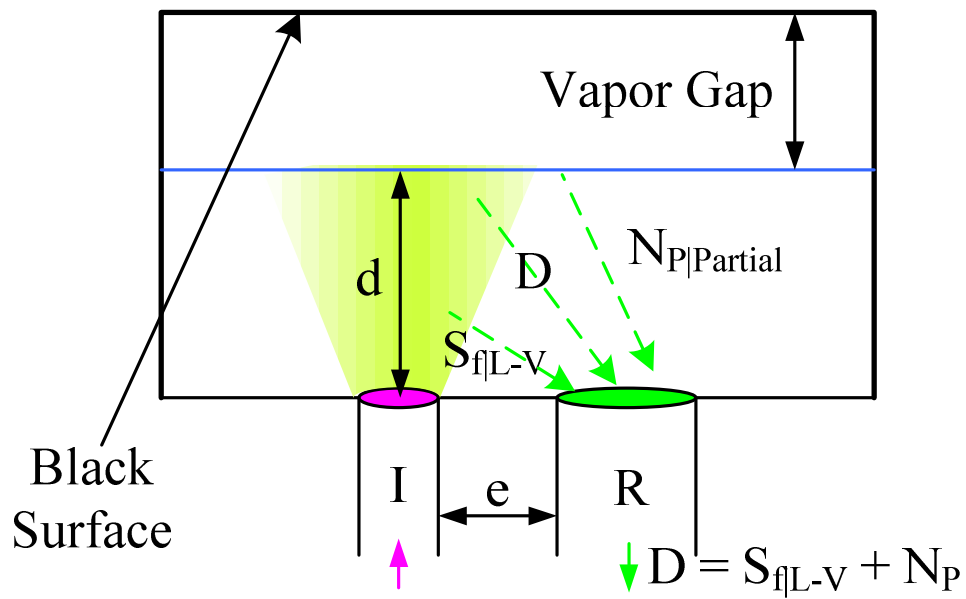


Figure 9a

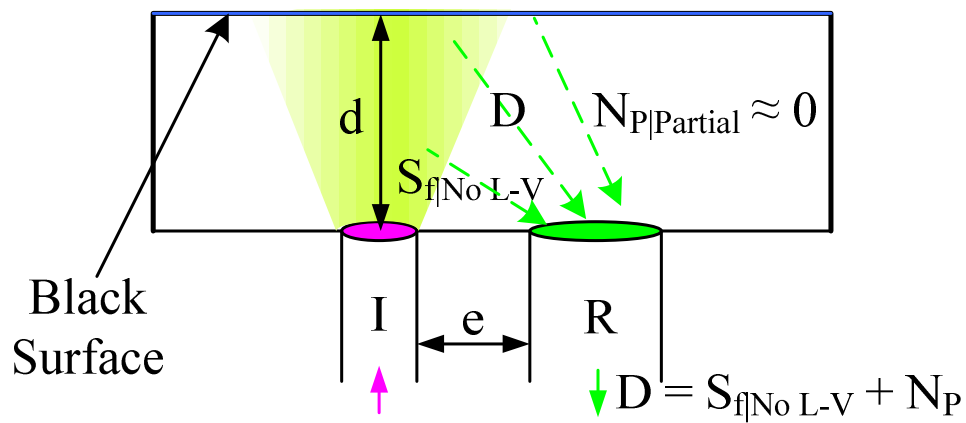


Figure 9b

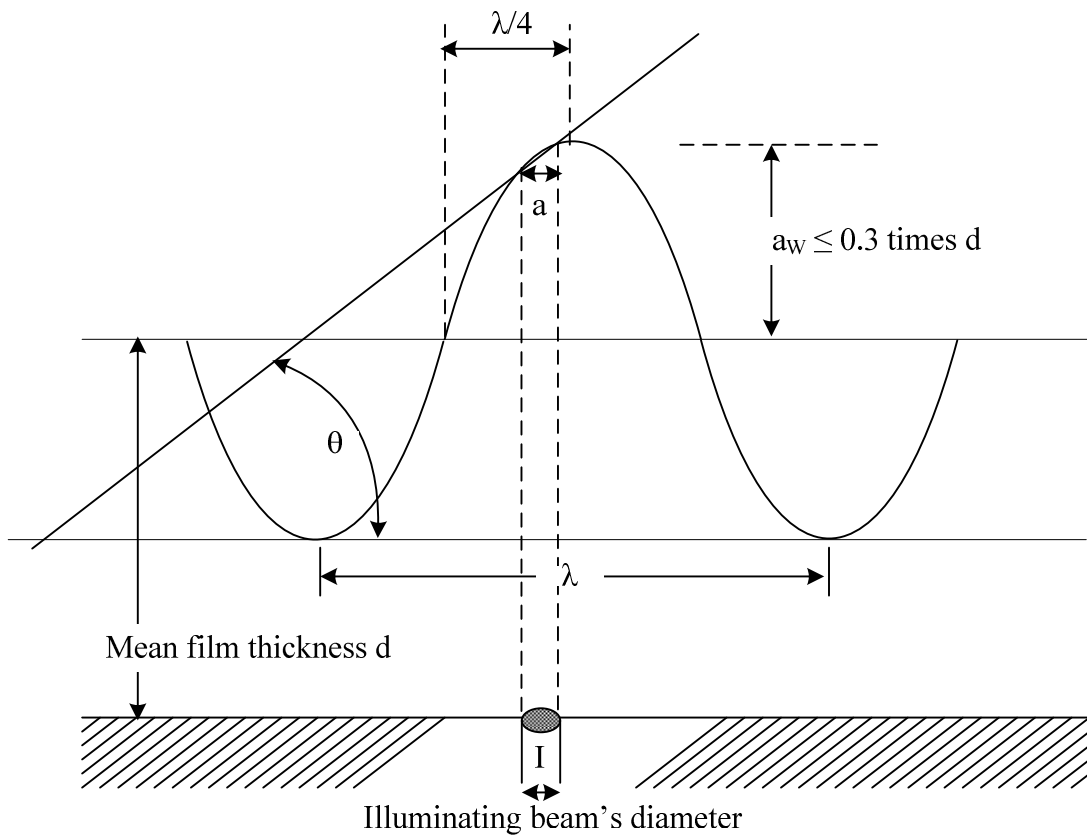


Figure 10

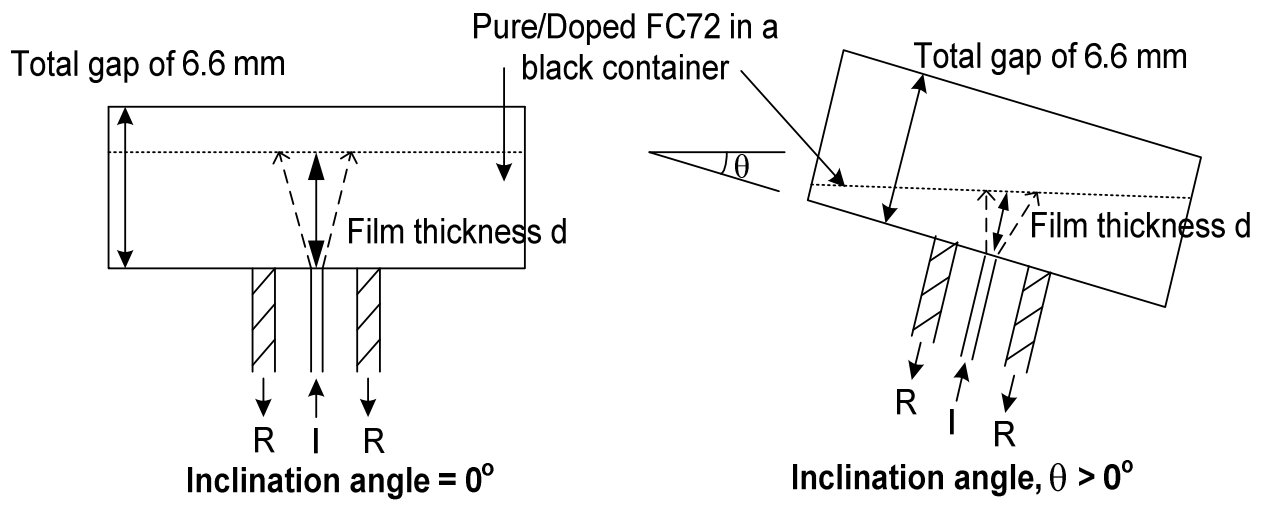


Figure 11

Optimum Setting (6 Receiving Fibers), 40.8 mA

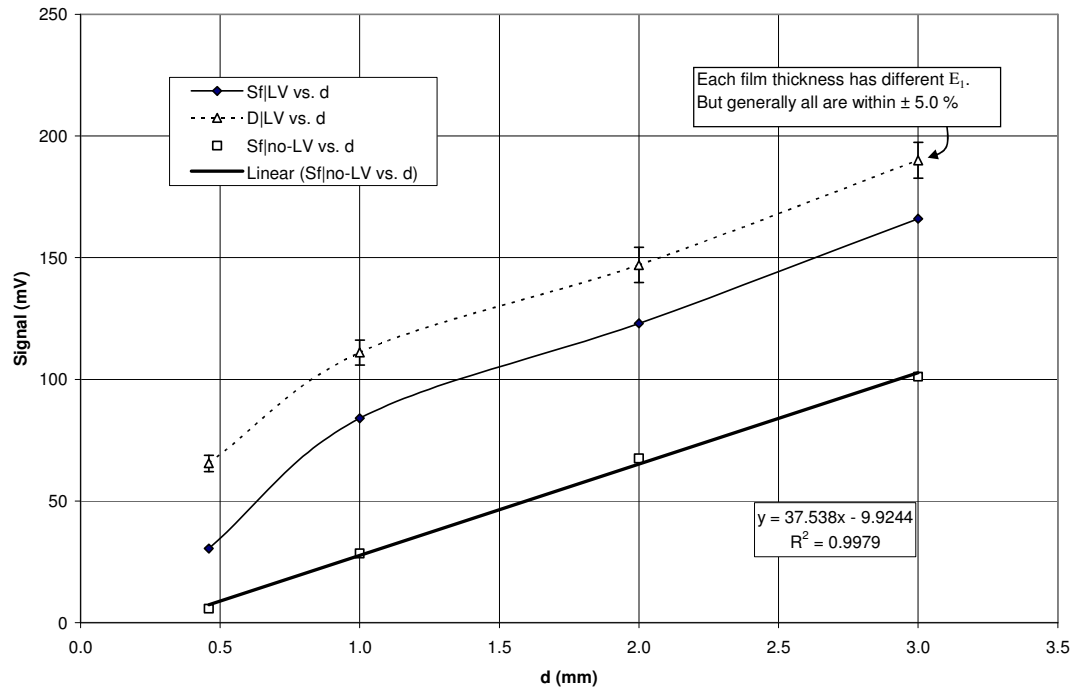


Figure 12

Optimum setting (with 6 receiving fibers), 40.8 mA

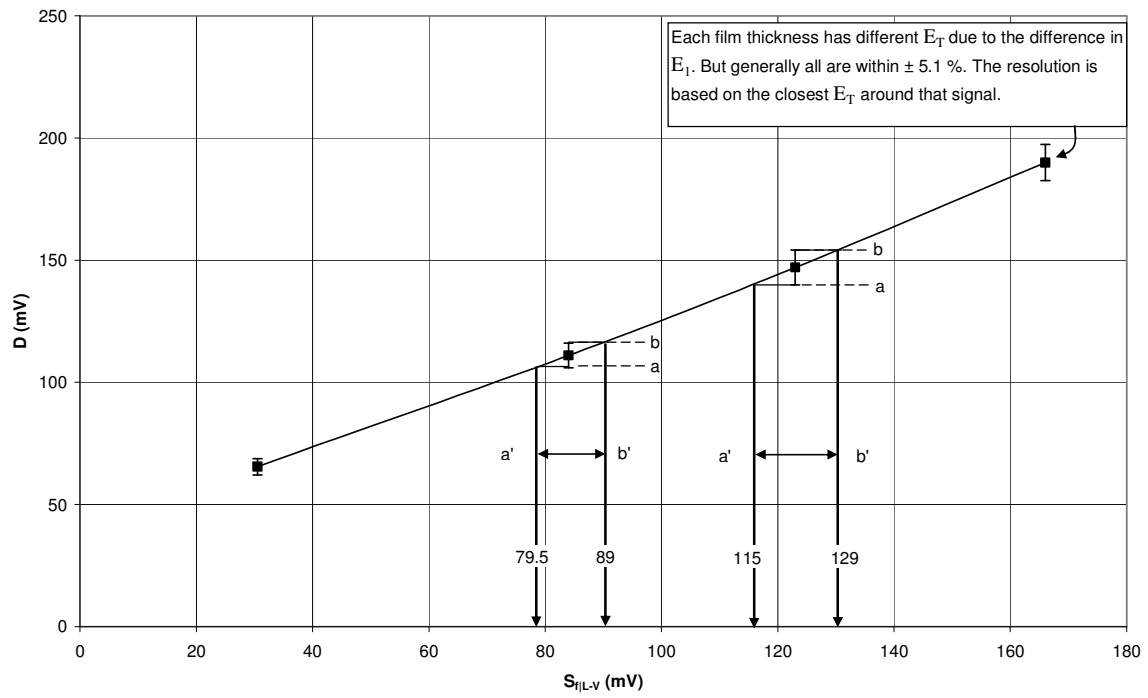


Figure 13

Optimum setting (with 6 receiving fibers), 40.8 mA

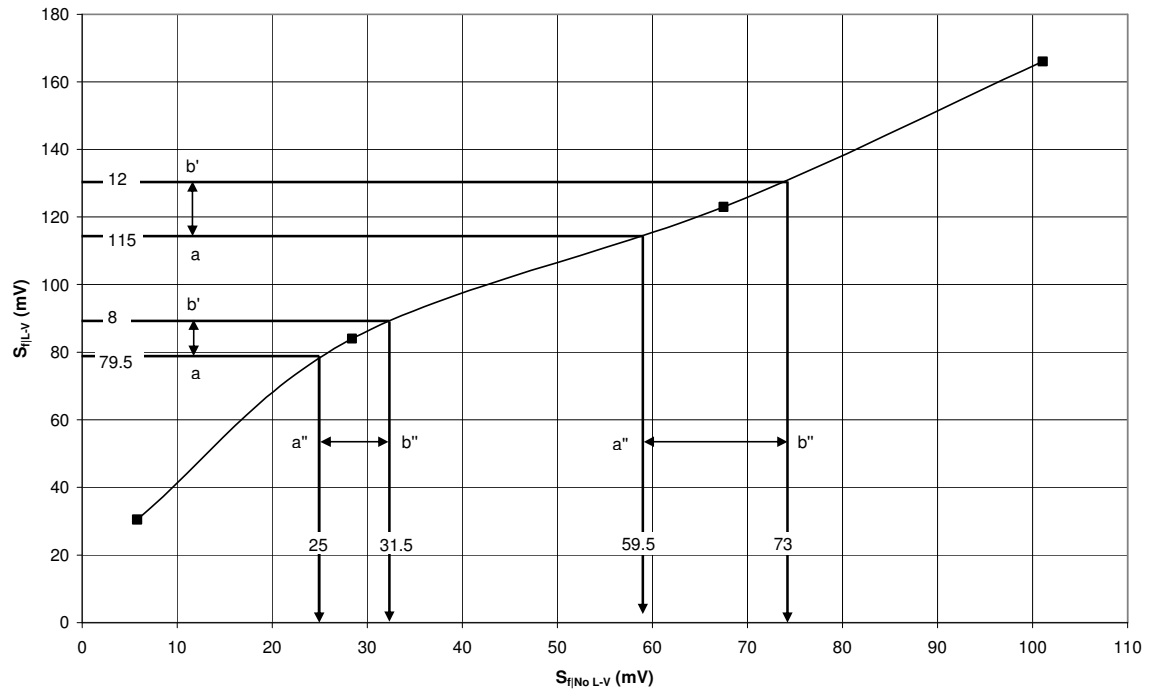


Figure 14

Optimum setting (with 6 receiving fibers), 40.8 mA

$$y = 37.538x - 9.9244$$

$$R^2 = 0.9979$$

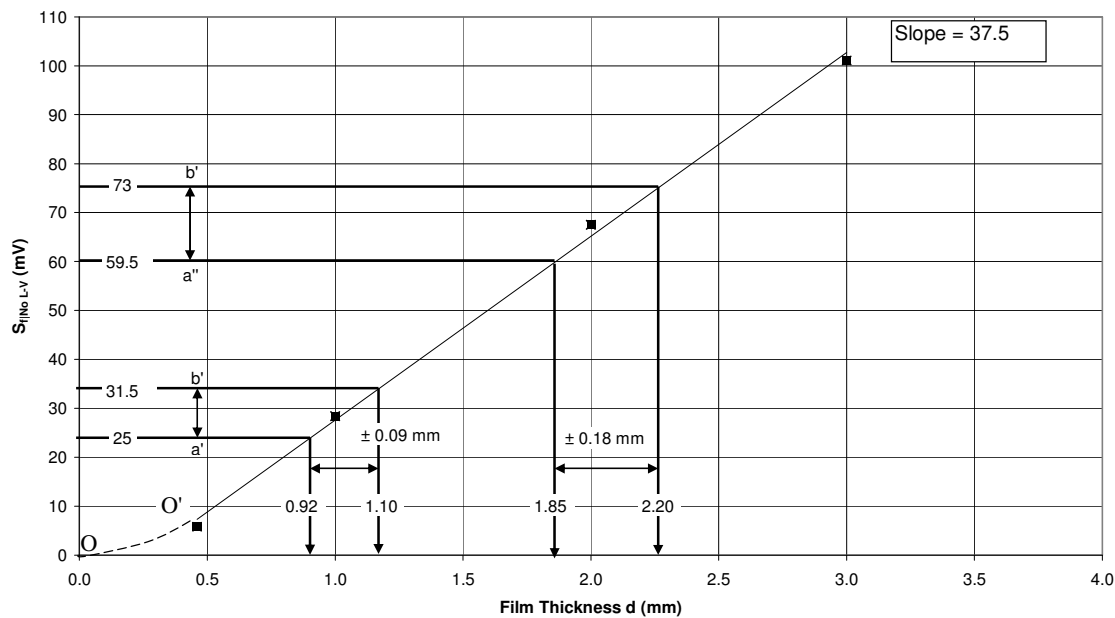


Figure 15

**460-480BP+blocker (diff. sides)
L/V interface - 45 mA, Single Probe**

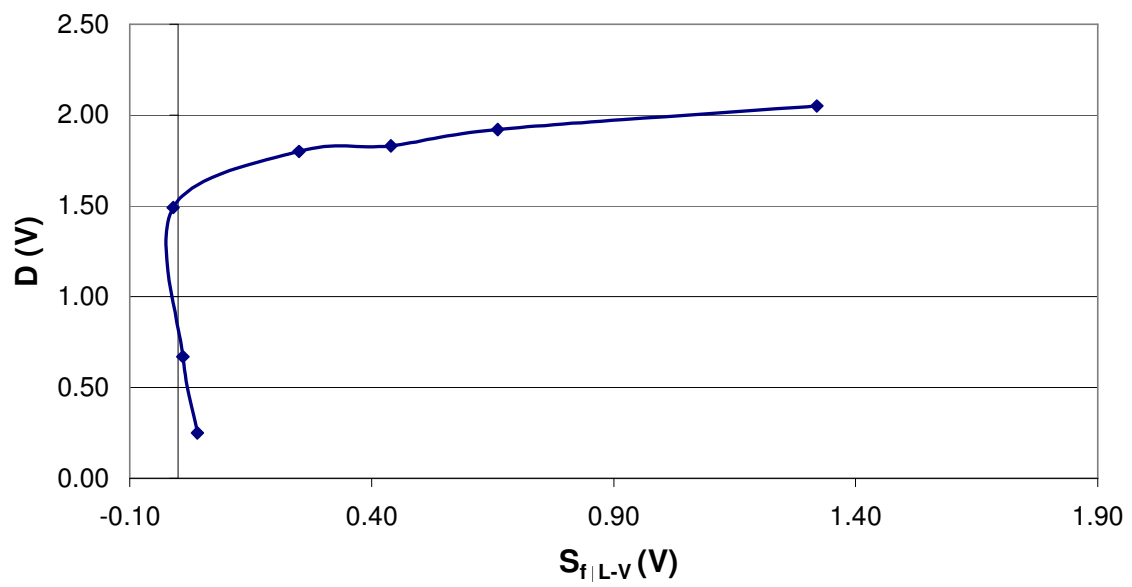


Figure 16

Concentration Effect at Temp. = 20°C, Optimum Setting

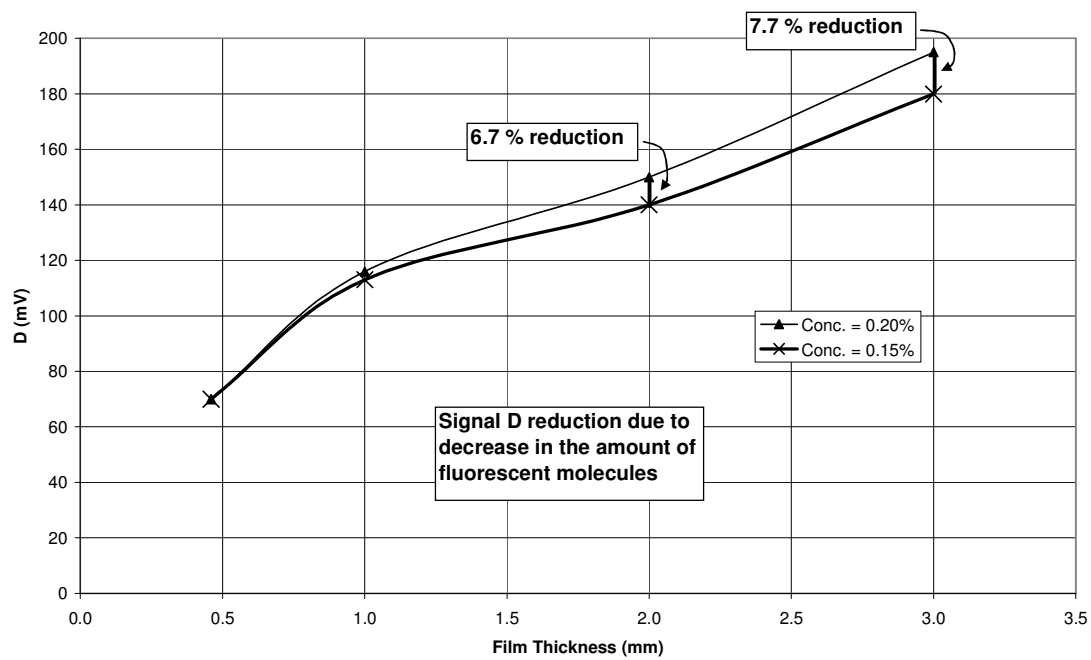


Figure 17

Temperature Effect at Conc. = 0.20%, Optimum Setting

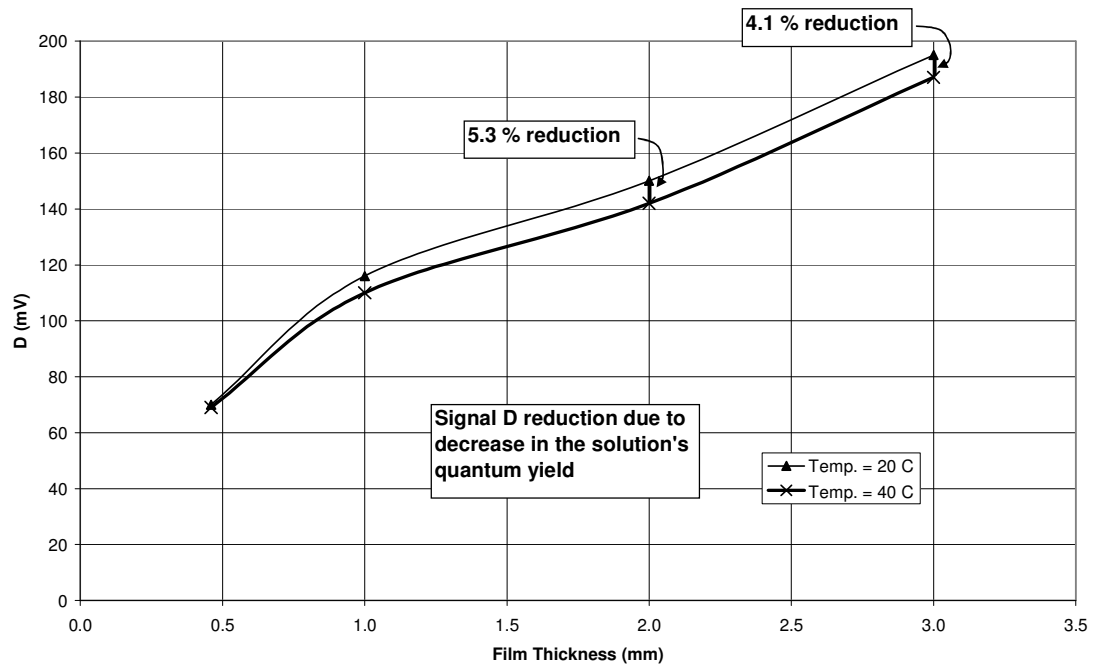


Figure 18

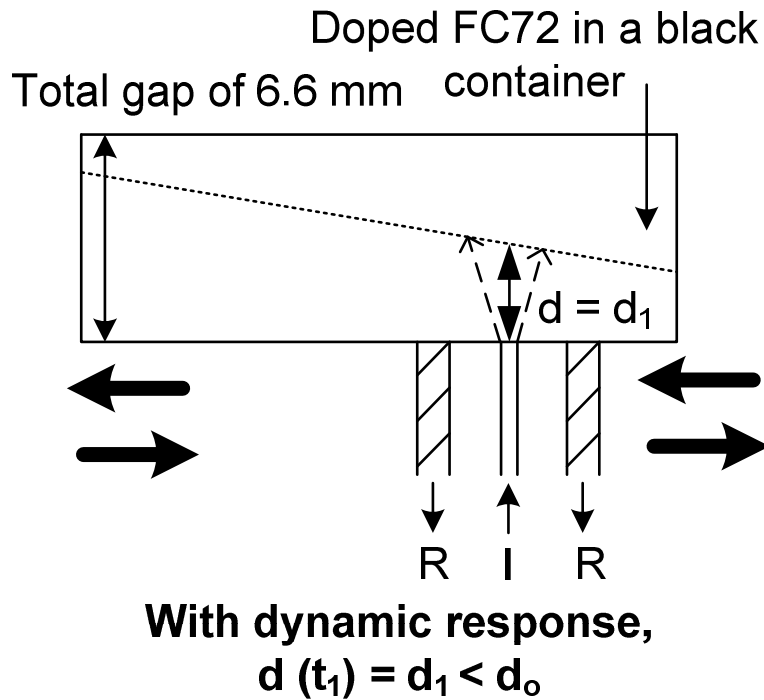
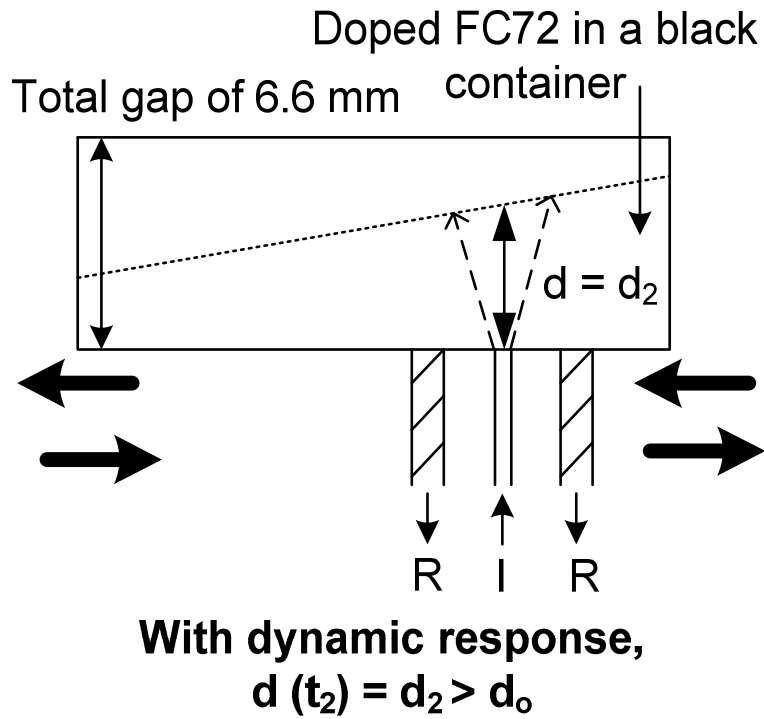


Figure 19

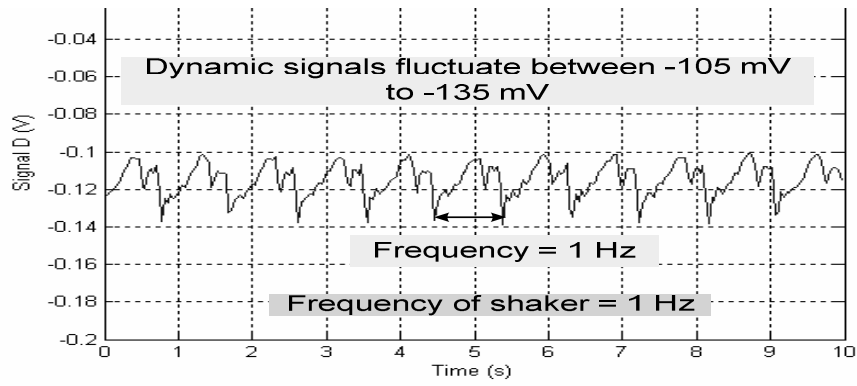


Figure 20a

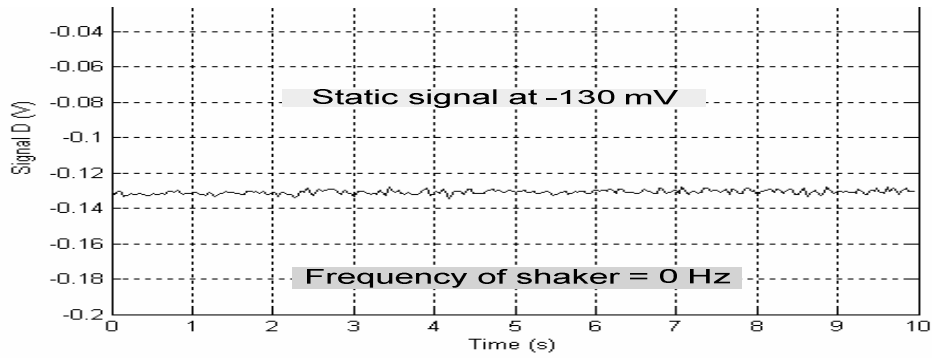


Figure 20b

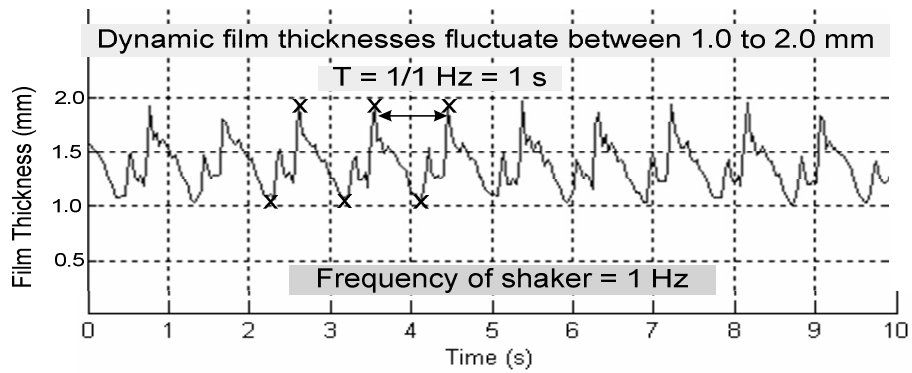


Figure 20c

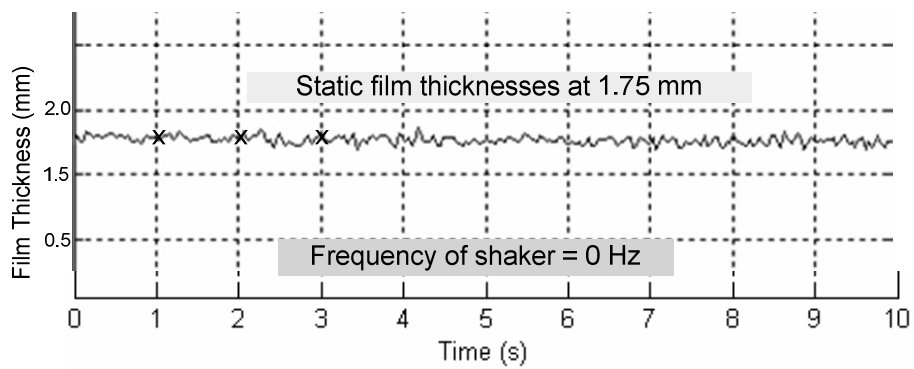


Figure 20d